# Neurogenic induction by Ngfr reduces reactive astrocytic Lcn2/Slc22a17 signalling, amyloid deposition and Tau phosphorylation

Tohid Siddiqui[1] (tohid.siddiqui@dzne.de), Mehmet Ilyas Cosacak[1] (mehmet.cosacak@dzne.de), Stanislava Popova[1] (stanislava.popova@dzne.de), Prabesh Bhattarai[1,2] (pb2886@cumc.columbia.edu), Ismael Santa-Maria[3,4] (is2395@cumc.columbia.edu), Giuseppe Tosto[2,3] (gt2260@cumc.columbia.edu), Caghan Kizil[1,2,3,*] (ck2893@cumc.columbia.edu)

[1] German Center for Neurodegenerative Diseases (DZNE) within Helmholtz Association; 01307, Dresden, Germany

[2] Department of Neurology, Columbia University Irving Medical Center; New York, NY 10032, USA

[3] Taub Institute for Research on Alzheimer's Disease and the Aging Brain, Columbia University Irving Medical Center; New York, NY 10032, USA

[4] Department of Pathology and Cell Biology, Columbia University Irving Medical Center; New York, NY 10032, USA

*Corresponding author: ck2893@cumc.columbia.edu

## Abstract

Defects in neurogenic ability in humans could be a culprit of the etiology of Alzheimer's disease (AD). Enhancing the neurogenic outcome in humans could enhance resilience to counteract neurodegeneration. However, molecular mechanisms that enhance neural stem cell neurogenic potential are largely unknown. We previously showed that zebrafish uses nerve growth factor receptor (NGFR) signalling to enhance pathology-induced neurogenesis. Here, we show that induction of NGFR signalling in mouse astroglia also induce proliferative and neurogenic capacity in the APP/PS1dE9 AD mouse model. Single-cell transcriptomics, spatial proteomics, and functional knockdown experiments showed that NGFR suppressed reactive astrocyte marker Lipocalin-2 (Lcn2). Blockage of Lcn2 receptor, Slc22a17, recapitulated the neurogenic effects of NGFR, and long-term NGFR expression reduced amyloid plaques and Tau phosphorylation. Immunostaining on postmortem human hippocampi with AD or primary age-related Tauopathy and 3D human astroglial cultures showed elevated LCN2 levels correlate with gliosis. Our study link the regulatory role of an autocrine molecular mechanism in astroglia to the neurogenic ability and modulatory effects on pathological hallmarks of AD, supporting the promise of neurogenesis-oriented therapeutic approaches as potential clinical interventions for this disease.

## Keywords

Mouse, Alzheimer's disease, neurogenesis, nerve growth factor receptor, Lipocalin 2, transcriptomics, proteomics, 3D human astrocyte culture, post-mortem human brain, amyloid, Tau

## Introduction

Generation of new neurons in adulthood reduces with vertebrate phylogeny [38]. Neurogenic regions are spatially restricted in mammals, which limits the addition of new neurons to the existing circuitry. Generation of new neurons and continuous integration to the existing circuitry could contribute to the resilience and cognitive reserve of the brain [36, 43], which could affect the late-onset neurodegeneration. Reduced neurogenic output was associated with the etiology of neurodegenerative diseases, as recent studies showed declining neurogenesis in Alzheimer's disease (AD) patients [33, 39]. Although it is not yet clear whether reduced neurogenesis is one of the culprits of AD, therapies aiming at enhancing neurogenic output hold promise for reverting the age-related neurodegenerative conditions. However, the molecular mechanisms by which neurogenesis could be therapeutically enhanced are largely unknown.

The disparity of the neurogenic ability within vertebrates has immense ramifications in the regenerative capacity of the central nervous system. Zebrafish has a widespread regenerative ability in its adult brain, which is unparalleled in the vertebrate clades [15, 25]. Astroglia that act as neural stem/progenitor cells are one of the key cell types for neuronal regeneration[23]. We generated an Alzheimer's disease model in adult zebrafish brain and found that a complex set of cellular crosstalk leads to production of more neurons despite the disease pathology [5-7, 14]. This model has strong parallelism to human AD brains in terms of molecular programs affected by AD pathology [12] and helped identify the functional relevance of genes associated with AD in humans [26, 28]. The extraordinary regenerative ability of astroglia in AD-like conditions in zebrafish rely on molecular mechanisms, one of which is the imposed neurogenic activity through the expression of nerve growth factor receptor (NGFR) [5, 13]. NGFR is not detected in mouse hippocampal astroglia, and we hypothesized that ectopic expression of NGFR could alter the neurogenic properties and AD pathology in mouse brain. In this study, we present the positive effects of NGFR signalling on reducing the AD pathology when activated in the astroglia of the mouse model of AD.

## Results

To express NGFR/p75NTR in the astrocytes of the subgranular zone (SGZ) of mouse dentate gyrus (DG), we generated lentiviral constructs that code for mCherry (control, Lv13) and mCherry and mouse NGFR (Lv16) (Fig. S1). These viral particles have enhanced efficiency for targeting astroglia as documented before [31]. Microinjection into mouse SGZ (Fig. 1A) results in efficient targeting and transduction (Fig. 1B). In control DG, NGFR is expressed at the periphery of the DG but not in SGZ, while Lv16 transduction leads to ectopic expression (Fig. 1B). The expressed receptor is functional as one of the NGFR ligands - BDNF - increases the proliferation of mouse DG astrocytes only when NGFR is expressed (Fig. S1C, S1D).

To determine the molecular programs that are altered after NGFR expression in astrocytes, we performed single-cell transcriptomics by dissecting the DG from Lv13 and Lv16-transduced wild-type mouse brains (Fig. 1C, 1D, Fig. S1E). Clustering the cell types and plotting Lv16-dependent expression of NGFR-mCherry (Fig. 1C-E) revealed that Lv16 transduction largely targets the astrocytes. Differentially expressed gene (DEG) (Data S1) and pathway analyses (Data S2 and Data S3) showed that NGFR expression reduced the pathways related to neurodegenerative diseases including AD while induced pathways related to sustained homeostasis and growth, such as proteasome, mTOR signaling and cell cycle (Fig. 1F). Analyzing the DEGs in astrocytes, we

found a general reduction in astrocytic markers that are associated with reactive or non-neurogenic states (e.g.: *Gfap, Apoe, Hopx, Ndrg2, Aldoc, Id3*) and an increase in the expression of genes associated with proliferation and differentiation (e.g.: *Prdm2, Enc1*, *Egfr, Mcm7, Cdk13*) (Fig. 1G-I), suggesting that NGFR signaling could promote proliferation and neurogenesis in mouse DG astrocytes.

To determine whether NGFR expression in DG astrocytes would enhance proliferation and neurogenesis, we performed Lv13 and Lv16 transduction, BrdU labeling, and quantified the extent of labelled astrocytes (GFAP+) and newborn neurons (Dcx+) at 3 days after transduction in wild type and APP/PS1dE9 mouse model of AD (Fig. 2, Fig. 3, and Fig. 4). We found that NGFR expression enhanced proliferation and neurogenesis in both healthy (Fig. 2A-F, Fig. 3, and Fig. 4; Data S4; by 2.99-fold and 2.08-fold, respectively) and AD mouse brains (Fig. 2G-L, Fig. 3, and Fig 4; Data S4; by 4.85-fold and 7.32-fold), validating the NGFR-mediated molecular changes in astrocytes (Fig. 1).

To determine the underlying mechanism of the effect of NGFR on proliferation and neurogenesis in astrocytes, we selectively analyzed the NGFR-transduced astrocytes in our single-cell sequencing by in silico dissection of NGFR-mCherry expressing cells and determining the DEGs in comparison to non-transduced astrocytes from the same mouse brain (analysis 1) or astrocytes from control virus (Lv13) transduced mouse brain (analysis 2) (Fig. 5A, Data S2 and Data S3). When we selected the top-50 DEGs and selected the common hits in analyses 1 and 2, we found 10 genes that changed their expression only upon NGFR expression (Fig. 5A). We hypothesized that if a specific cell autonomous effect of NGFR is running through a select number of genes in neurogenic cell populations, then those genes could be mainly expressed in astrocytes. To determine whether any of the identified candidate genes has restricted astrocytic expression, we generated tSNE plots and found that *Gm8251, Cxcl1*, and *Lcn2* have a predominant astrocytic expression (Fig. 5B). By drawing Vln plots, we observed that only *Lcn2* showed a significant change in expression in astroglia (Fig. 5C). To validate our findings, we performed immunohistochemical staining for Lcn2 in Lv16-transduced DG and found that while non-transduced astrocytes were Lcn2-positive, NGFR-mCherry positive astrocytes did not express Lcn2 (Fig. 5D), supporting that NGFR signalling specifically reduces Lcn2 in DG astrocytes.

Lcn2 is a ligand and can bind to two receptors, Lrp2 and Slc22a17 [4, 21]. To determine whether these receptors are expressed in mouse DG, we plotted tSNE plots for the two receptors and found that *Lrp2* is not expressed in DG while *Slc22a17* expression is observed in astrocytes (Fig. 5E), suggesting that Lcn2 can act as an autocrine signalling on astrocytes. To determine whether Lcn2 can alter the proliferation of astroglia, we injected Lcn2 into the hippocampus of the healthy mice, treated the animals with BrdU and analyzed the labelled astroglia (Fig. 5F). We observed that Lcn2 significantly reduces the number of label retaining GFAP cells, indicative of reduced proliferation (Fig. 5G). To determine whether Lcn2-Slc22a17 signalling is biologically relevant to neurogenesis, we performed loss of function studies for *Slc22a17* (Fig. 5H-J) by using morpholino oligonucleotides that effectively reduce Slc22a17 protein levels (Fig. S2B-D). Since Slc22a17 is expressed in several cell types and to avoid pleiotropic effects of the loss-of-function that would confound the observations, we transduced the mouse DG astrocytes *in vitro,* treated the cells with *Slc22a17* morpholinos and then transplanted the astrocytes to the SGZ of wild type mouse brains (Fig. 5H). With this method, specific blockage of Lcn2-Slc22a17 signalling in mCherry-positive

astrocytes could be assessed. To determine the progeny of the transplanted astrocytes, we injected the mice with BrdU after transplantation. After performing immunohistochemical staining for BrdU (newborn cells), Dcx (early neurons) and mCherry (transduced cells), we found that compared to Lv13 and control morpholino, Lv13 and Slc22a17 morpholino significantly increased the generation of newborn neurons from transplanted astrocytes and this increase is comparable to Lv16 (NGFR) transduction alone (Fig. 5I, J; Data S4). These results suggest that the imposition of neurogenic potential by NGFR receptor expression to DG astrocytes is through autocrine Lcn2-Slc22a17 signalling.

Since NGFR signalling in DG astrocytes induced proliferation and neurogenesis (Fig. 2), and suppressed the molecular pathways related to AD (Fig. 1), we hypothesized that active NGFR signalling could alter the pathology of AD, as recent studies correlated reduced neurogenesis to the disease pathology [2, 10, 11, 24, 33]. To determine whether NGFR signalling would alter AD-related proteins that cannot be identified by transcriptomics, we performed spatial proteomics on mCherry-enriched regions of Lv13 and Lv16-transduced SGZs of wild type and APP/PS1dE9 AD model (Fig. 6A). After data normalization and quality control by pairwise comparison of normalization parameters (Fig. S3, Data S7 and Data S8), we plotted the fold changes in protein expression levels between NGFR and control transduction (Fig. 6B, Fig. S4 and Fig. S5). We found that the highest fold changes upon NGFR transduction in APP/PS1dE9 mouse was observed for Aldh1l1 (-63% in wt, -53% in APP/PS1), amyloid beta-42 (-21% in wt, -47% in APP/PS1), phosphorylated Tau (S199) (-86% in wt and-75% in APP/PS1), phosphorylated Tau (S214) (-40% in wt, -54% in APP/PS1), and BAG3 (-39% in wt, -61% in APP/PS1) (Fig. 6B). Other AD-related proteins such as pTau-S396, pTau-S404, and APOE were also downregulated by NGFR (Fig. 6B, Data S8), suggesting that activation of NGFR signalling in DG astrocytes could ameliorate the AD pathology. To test this hypothesis, we transduced the APP/PS1dE9 mice with Lv16 and analyzed these brains 6 months after transduction (Fig. 6C). mCherry signal in the transduced hemisphere covered the entire DG, indicating that NGFR-transduced astrocytes contributed to neurogenesis (Fig. 6D). Additionally, when we analyzed different subregions of the hippocampus, we observed reduced immunoreactivity for 4G8-positive amyloid plaques upon NGFR (Fig. 6E), and this reduction amounted to 22% in the entire hippocampus (Fig. 6F). Since spatial proteomics showed reduced levels of phosphorylated Tau (Fig. 6B), we tested these findings by performing immunohistochemical staining for pTau-S199 in control and NGFR-transduced hemispheres of APP/PS1dE9 mouse DG. We observed that NGFR-transduced DGs have significantly lower amounts of pTau-S199 in the overall hippocampus (11%, Fig. 3G, H), while the difference in SGZ is more pronounced (Fig. 6G). In overall, these results suggest that NGFR signalling could reduce the amyloid and Tau pathology by enhancing neurogenesis in mouse hippocampus.

To determine whether NGFR receptor expression in human brains would correlate with proliferating cells, we analyzed three publicly available single-cell sequencing datasets (human brain organoids, fetal human brain, adult human brain) (Fig. S5) [18, 22]. Cell clustering, marker gene identification, and cell type determination followed by generation of tSNE plots for NGFR and PCNA (proliferating cell marker) showed that in brain organoids and developing fetal brain, NGFR expression partially overlaps to proliferating astroglial cells while in adult human brains, NGFR is not expressed in astroglia (Fig. S5), suggesting an age-related loss of NGFR activity might correlate with reduced neurogenesis.

Finally, we hypothesized that the expression of *LCN2* could increase in the brains of AD patients, where neurogenesis is reduced. To test this hypothesis, we performed immunolabeling of human hippocampi for GFAP and LCN2 in healthy controls and AD patients (Fig. 7). We found that in healthy aged individuals, scarce LCN2 expression is observed (Fig. 7A, B) while in human brains with clinical/pathological AD, LCN2-positive astroglia increases dramatically concomitant to architectural changes of glial extensions and elevated hypertrophic astrocytes (Fig. 7C, D). Quantification of LCN2-positive GFAP cells normalized to the overall GFAP cells indicate that the number of LCN2-positive glia increases significantly in late-stage AD patients (Braak stage V-VI) but not in earlier stage AD (Braak stage IV-V) (Fig. 7E). We observed that the LCN2-expressing astroglia in human brains are more compact than their healthy counterparts (Fig. 7B, D). To determine whether LCN2 is sufficient to alter the morphology of astroglia, we used 3D hydrogel cultures of primary human astrocytes (Fig. 7F). We observed that treatment of astroglia with LCN2 significantly reduces the glial volumes indicative of a reactive state (Fig. 7G).

**Discussion**

Reduced neurogenic outcome in Alzheimer's disease could be a pathological culprit of the disease [2, 33, 39]. Therefore, enhancing the neurogenic outcome in disease conditions could help to restore the brain's resilience and ability to cope with neurodegeneration [11, 24]. However, the understanding of the molecular mechanisms of such a neurogenic competency is insufficient. Previous studies showed that neurotrophin signalling, especially BDNF, imposes a neuroprotective ability [20, 47] and can contribute to the amelioration of cognitive decline in AD [8, 10]. Major neurotrophin receptor TrkB was associated with neuronal survival; however, BDNF is not directly inducing neural progenitor proliferation and neurogenesis in rodent brains [10]. However, we previously showed that BDNF signalling imposes neuroregenerative ability through directly inducing astroglial proliferation and neurogenesis in an experimental adult zebrafish brain model [5]. We found that this activity is dependent on NGFR/p75NTR receptor but not TrkB. NGFR can be bound by various ligands such as BDNF or NGF or their pro forms [34]. In the hippocampus, we did not detect active cleaved forms of BDNF or NGF in the SGZ, but pro-BDNF is expressed in this region (Fig. S6). This is consistent with the binding ability of pro-BDNF to NGFR [16], and suggests that NGFR/pro-BDNF signalling could be responsible for neurogenic activity of mouse astrocytes. Therefore, here we show that transferring the molecular understanding from organisms with neuroregenerative ability, such as zebrafish, to mammalian brains is a promising cross-species approach to study the neuroregenerative ability to counteract AD pathology.

We found that Lcn2 expression is negatively regulated by NGFR signalling in mouse astroglia, and Lcn2 and its receptor Slc22a17 negatively regulates astrocyte proliferation and neurogenesis. Lcn2 is a secreted protein that is associated with autocrine induction of reactive astrocyte state and induce hypertrophic GFAP expression [29]. Lcn2 is upregulated after several brain diseases such as stroke and may contribute to neurodegeneration, promote cell death and inflammation [49]. In this study, we found that Lcn2 is also upregulated in AD, consistent with previous findings [30]. However, the link between NGFR signalling in astrocytes and Lcn2 was not documented. We propose that NGFR signalling specifically downregulated Lcn2 and promote neurogenic route rather than reactive astrocyte direction. Our spatial proteomics and single-cell transcriptomics data support this hypothesis (Fig. S6, Data S6). Additionally, our spatial proteomics analyses showed that among the immune-related proteins, CD44 was the most highly downregulated after NGFR

expression (Fig. S4), which is consistent with previous findings that Lcn2 promoted CD44 expression [45].

We propose that NGFR signalling is an evolutionary determinant of the neurogenic potential of the astrocytes. In zebrafish, NGFR signalling is naturally active in neural progenitor cells throughout the lifespan, which correlates with the life-long proliferation and neurogenic activity [5], while in the mouse brain, NGFR is not present in hippocampal astrocytes. When NGFR is activated, reactive astrocyte programs are suppressed through suppression of Lcn2 and neurogenic programs prevail. Therefore, mammalian brains could have lost NGFR expression in adult brain astrocytes through the evolution, and this could have restricted the neurogenic outcome in health and disease in mammalian brains. This hypothesis is supported by findings that a small population of astrocytes (0.3%) in the subventricular zone (SVZ) of mouse astrocytes are NGFR-positive and they constitute a highly proliferative and neurogenic subset [48], and NGFR signalling could regulate genes related to cell proliferation, differentiation and neurite growth in vitro [1]. Our findings on single-cell sequencing analyses of human brain organoids, fetal human brain, and adult human brains (Fig. S5) also validated the notion that NGFR expression in astrocytes is declining with age and could contribute to the hampered neurogenic outcome or inability of adult human brains to fulfil efficient neuroregeneration. In AD patients, LCN2-positive astroglia increase (Fig. 7), suggesting that NGFR/LCN2/SLC22A17 signaling axis could be a critical fate determination step between neurogenic versus reactive gliotic response in disease. In primary age-related Tauopathy, LCN2 expression does not change significantly in astroglia (Fig. S6), which support the findings that amyloid toxicity could be the cause of LCN2 misexpression and subsequent AD pathology including the Tau phosphorylation. pTau-S199 is a critical residue that is phosphorylated by Cdk5 at late stages before the neurofibrillary tangle formation and is one of the residues detected by AT8 immunostaining [32]. The reduction in Amyloid beta42 and phosphorylated forms of Tau protein could explain the long-term benefit of active NGFR signalling in astrocytes.

It is unclear how the neurogenic effects of NFGR, anti-reactive gliotic role for the suppression of *Lcn2* expression, and other NGFR-mediated mechanisms act in concert to alleviate the pathological hallmarks of AD in long-term. Our single cell transcriptomics comparing NGFR-transduced brains versus controls showed that in neuronal, microglial and oligodendrocyte cell populations, molecular pathways related to unfolded protein response, clearance of misfolded proteins, protein processing, proteasome and Tau protein binding were enriched (Fig. S7). This suggests that NGFR signalling may induce more efficient clearance of toxic proteins, which might explain the long-term reduction of amyloid and Tau burden in NGFR-transduced mouse brains (Fig. 6). This is consistent with previous findings [44]. Recently, we identified that astroglial end-feet need to be retracted from the blood vessels to enhance efficient clearance of amyloid aggregates, and genetic mutations in humans alter this ability [28]. While astroglia undergo proliferation, they retract their end-feet [9, 17, 27, 44, 46] and this could help enhance clearance. Longitudinal studies in animal models of AD and in human AD cohorts could help scrutinize on this aspect in future. Finally, our study identified Slc22a17 as a potential drug target to design therapies for interventions that will aim to enhance neurogenesis in AD.

Our study is strong in terms of providing a mechanistic link between neurogenesis and reduced AD pathology. Additionally, we provide an evolutionarily conserved mechanism for NGFR

signalling (from zebrafish to mammals) in regulating neurogenesis-related pathological alterations. We provide evidence from two mammalian species – human and mouse – for the antagonistic effects of NGFR signalling on LCN2 and reactive gliosis. Our study utilized transcriptomics, spatial proteomics, in vivo functional knockdown studies, cell labeling and tracing as sensitive tools and identified a potentially druggable receptor, Slc22a17. Our study has also limitations. We performed transient knockdowns in vivo, and transgenic animal models can be used in the future for measuring the sustained effects. Additionally, in the future, Tau pathology models in mouse can be used to determine the long-term effects of neurogenesis and NGFR signalling on Tauopathies. Finally, we used a ubiquitous promoter for the viral gene expression because we sought for tracing the transduced cells for long-term. Therefore, astrocyte specific promoters would not be feasible. Our initial transduction mainly labels astrocytes, but we cannot exclude that the nearby cells could also be transduced. Based on our observations, this ratio is rather low and would not affect our conclusions drawn, yet in the future, cre-lox based cell specific recombination strategies could be employed for cell-specific recombinations.

**Conclusions**

We provide evidence that induced neurogenesis can alter Alzheimer's disease (AD) pathology in mammalian brains. We previously identified the nerve growth factor receptor (NGFR/p75NTR) signalling as a key mechanism for Alzheimer's disease-induced neuroregeneration in adult zebrafish brain model of AD-induced neuroregeneration. Here, by using mouse models of AD, virus mediated gene expression, gene knockdown and transplantation, single cell transcriptomics, spatial proteomics, immunohistochemical investigation of mouse brains and post-mortem human brain tissue, we show that expression of NGFR in mouse hippocampal astroglia that are normally devoid of this receptor induces proliferation and neurogenesis. We discovered an autocrine molecular mechanism - Lipocalin-2 (LCN2) / Solute carrier protein 22a17 (Slc22a17) ligand receptor interaction regulates the neuroregenerative activity of astroglia by controlling the neurogenic versus reactive states. In long term, NGFR-induced neurogenesis reduces amyloid pathology and Tau phosphorylation, which are two major hallmarks of AD. We found that in humans, LCN2 expression is elevated in AD and primary age-related Tauopathy patient brains, indicating a relationship between reduced neurogenic capacity and the etiology of these diseases. By using the single cell sequencing datasets, we also show that in fetal human brains, 3D brain organoids and human AD patient brains, NGFR expression defines neurogenic capacity that declines with age.

Our results support the neurogenic hypothesis in AD and provide mechanistic evidence that reduced neurogenic outcome is a pathological culprit of the disease. We described a molecular mechanism that negatively correlates with neuroregenerative capacity in mammalian brains and showed that enhanced neurogenesis could counteract age-related AD pathology. We also propose that evolutionary determinants of neuroregenerative potential can be identified by cross-species comparison, and engineered induction of regenerative programs could help design novel therapeutic routes in AD in humans. Our study also identified Slc22a17 as a potential drug target to design therapies for interventions to enhance neurogenesis in Alzheimer's disease.

## Materials and Methods

Animal Maintenance

Mice were kept under pathogen-free conditions on a strict 12 hour alternating light and dark cycle with standard mouse food (chow) and water *ad libitum*. They were group-housed in standard ventilated cages prior to the experiments and were kept in individual cages after surgical procedures. Fixed gender mice, aged between 52-56 weeks were used for the experiments unless stated otherwise. B6.Cg-Tg(APP695)3DboTG(PSEN1dE) mice were obtained from Jackson Laboratories (Bar Harbor, ME, USA) and were maintained as a heterozygous breeding colony.

Lentiviral Construct and production

In this study, we have designed and used p6NST90-hUb-mNGFR-T2A-mCherry-Lv16 (Lv16) and p6NST90-hUb-mCherry-Lv13 (Lv13) for lentiviral production (Fig. S1). These lentiviral plasmids were constructed using a second-generation HIV based lentiviral system, comprising of 3 plasmids, a) p6NST90 - transfer vector plasmid that contains the gene of interest (mNGFR and mCherry) [19, 37]; b) pCD/NL-BH - packaging plasmid that contains the Gag, Pol, Rev and Tat genes; and c) pczVSV-Gwt - envelope plasmid that encodes the VSV-G protein. Mouse NGFR under the mammalian promoter from the human ubiquitin C gene and mCherry, separated by T2A, were cloned in the backbone of the HIV transfer vector to generate the Lv16 construct. Similarly, Lv13 was constructed without mouse NGFR as a control vector (see table S1 for primer details).

To produce viral particles, we co-transfected the packaging cells (HEK293T cells) with the vectors pczVSV-Gwt and pCD/NL-BH and the transfer vector p6NST90, in a 10 cm dish with 8 ml of DMEM (10% heat-inactivated FBS, 1% Pen/Strep), 18-21 dishes per condition. 5 µg of each plasmid was mixed in 1 ml prewarmed blank DMEM (without FBS and pen/strep) and combined with 1 ml of blank DMEM containing 45 µl of polyethylenimine (PEI) before adding to the HEK293T cells. At 48 h post-transfection, the medium from the transduced cells was collected, filtered, and concentrated by several rounds of ultracentrifugation. The presence of mCherry expression was verified by fluorescent microscopy.

Primary human astrocytes and mouse neural stem/progenitor cells culture

Primary human astrocytes (pHA) were purchased from ScienCell Research Laboratory (SRL, Catalog Number 1800) at passage one. Using complete astrocyte medium (SRL, Catalog Number 1801) supplemented with 5% fetal bovine serum (SRL, Catalog Number 0010), 1% astrocyte growth supplement (SRL, Catalog Number 1852), and 1% penicillin/streptomycin solution (SRL, Catalog Number 0503); pHA were sub-cultured to obtain passage two pHAs which were used for all experiments. Mouse neural stem/progenitor cells (NSPCs) were isolated from the dentate gyri of 3-month-old WT mice as previously described [31, 41, 42]. Briefly, DGs were dissected out of the hemispheres of the freshly isolated adult mice brains on ice in PBS containing Pen/Strep. Using a scalpel, tissues were minced a little followed by enzymatic digestion with the Neural Tissue Dissociation kit from Miltenyi Biotec as per the manufacturer's instructions. Following the dissociation, the cell suspensions were cultured in PDL/Laminin coated 25 $cm^2$ flask using Neurobasal medium (GIBCO, Life Technologies), supplemented with 2% B27 (Invitrogen), 1x GlutaMAX (Life Technologies), 50 units/ml penicillin/streptomycin, 20 ng/ml EGF (Peprotech, AF-100-15), and 20 ng/ml FGF (Peprotech, AF-100-15). Cells were kept in an incubator with a

5% CO2/95% air atmosphere at 37ºC and media was exchanged every 48 h. Only passages 7-10 were used during the experiments.

Biohybrid-hydrogels 3D culture and lipocalin-2 treatment

Primary human astrocytes were encapsulated in biohybrid-hydrogels as previously described [35]. 10-µl hydrogels were created with a concentration on 4 million cells per ml (n=3) and were treated with 200 ng/ml lipocalin-2 or PBS in a complete astrocyte medium for one week. After two weeks of culture, hydrogels were fixed using 4% PFA and were stained for GFAP markers.

Generation of Lv13 and Lv16-transduced human astrocytes

Lv16-p6NST90-hUb-mNGFR-T2A-mCherry and Lv13-p6NST90-hUb-mCherry human astrocytes cell lines were generated using pHA pf passage 3 which were transduced with respective viral vectors. For transduction, pHA were seeded in a 24-well plate and were cultured until cells reached 70-80% confluency using a complete astrocyte medium. The respective viruses were then added to each well and cells are incubated for 24 hours at 37ºC in an incubator with a 5% CO2/95% air atmosphere. After 24 hours, the media is exchanged, and cells are allowed to grow until they were 90% confluence. Cells supernatant was checked for viral load after 72 hours of infection and virus particle-free cells were passaged to a bigger vessel. Cells from overall passages 6 were used for all experiments.

Slc22A17 and control morpholino of Lv13 and Lv16 mouse neural stem/progenitor cell lines

Mouse NSPCs from passage 7 were used to generate the Lv16-p6NST90-hUb-mNGFR-T2A-mCherry and Lv13-p6NST90-hUb-mCherry mouse NSPCs cell line. Mouse NSPCs were cultured in a PDL/Laminin coated 25 $cm^2$ flask at 10,000 cells per $cm^2$ concentration using Neurobasal plus medium (GIBCO, Life Technologies), supplemented with 2% B27 (Invitrogen), 1x GlutaMAX (Life Technologies), 50 units/ml penicillin/streptomycin, 20 ng/ml EGF (Peprotech, AF-100-15), and 20 ng/ml FGF (Peprotech, AF-100-15). Lv16 and Lv13 virus were then added to each flask and cells are incubated for 24 hours at 37ºC in an incubator with a 5% CO2/95% air atmosphere. Media was changed after 24 hours and cells are allowed to recover and grow until they were 70-80% confluence (approx. 4 days, media change at every 48 hours). 5uM of control and Slc22A17 morpholino oligos were added to respective cell line flasks and were incubated for 24 hours. Cells were washed after 24 hours with fresh media.

Stereotaxic injections of lentiviral vectors, lipocalin-2, and neural stem cells

The stereotaxic injection procedure was carried out as previously established protocol [3]. Briefly, during the entire surgery, the mice were anesthetized using a mix of oxygen and isoflurane (49:1) (Baxter – HDG9623) flow and placed on a pre-warmed heat-pad to prevent hypothermia. The head was immobilized with the help of ear bars and the eyes were with a protective ointment to avoid cornea dehydration. To minimize any possible pain after the surgery, an analgesic was subcutaneously injected prior to the procedure. The hippocampal injection coordinates were ± 1.6 mm mediolateral, −1.9 mm anterior-posterior, and −1.9 mm dorsoventral from the Bregma, where the virus was dispensed at 200 nl/min speed. After the injection, the capillary was slowly retracted, followed by the release of the ear bars and stitching of the injection site.

For the viral injections of p6NST90-hUb-mNGFR-T2A-mCherry-Lv16 (Lv16) or p6NST90-hUb-mCherry-Lv13 (Lv13), 1 µl of each virus was injected into either hemisphere. For the Lcn2

injection experiment, 1 µl of 10ng/µl Lcn2 solution was injected into the right hemisphere and 1 µl vehicle solution into the left. For the injection of morpholino-treated cells, after 24 hours of morpholino treatment cells were lifted using Accutase (Gibco, A11105-01), immediately followed by a cranial injection to avoid keeping them on ice for longer than 1 hour. Each hemisphere of WT mice was delivered with $1x10^5$cells/µl of cell suspension at a speed of 200 nl/min using the Nano-injector system. At 3 days post-injection, mice were sacrificed either via cervical dislocation followed by hippocampi extraction or via transcardial perfusion to isolate the whole brain for further processing.

BrdU labeling and tissue preparation

To label proliferating cells, mice were injected intraperitoneally (IP) with BrdU (50 mg/kg) 3 times on the day of cranial injection, 9 hours apart, followed by an IP every 24 hours until the end of experiment. Mice were sacrificed by an overdose of Ketamine/Xylazin (0.25 mL per 25 g of body weight) mixture and perfused transcardially with NaCl (0.9% w/v) followed by 4% paraformaldehyde (PFA). Brains were harvested and post-fixed in 4% PFA at 4ºC overnight. For cryopreservation of the fixed tissue, brains were transferred to a 30% sucrose solution for 2–3 days. Coronal sections with a thickness of 40 mm were cut using a sliding microtome (Leica SM2010) cooled with dry ice. Free floating sections were collected in 6 consecutive series and stored in cryoprotection solution (CPS; 25% ethylene glycol, 25% glycerol in 0.1 M phosphate buffer pH 7.4) at -20ºC. Every sixth section of each brain was pooled in one series for immunohistochemistry.

Fluorescence immunohistochemistry

Mouse: Prior to immunohistochemistry, the free-floating sections were washed in PBS 3 times, blocked in 10% Donkey or Goat Serum, 0.3% Tween 20, 1x PBS solution for one hour at room temperature. In the case of DCX and BrdU staining, antigen retrieval was performed in 2 N HCl for 30 min at 37ºC followed by 3x washing in PBS. Primary antibodies (4G8, Aldoc, BDNF, BrdU, DCX, GFAP, Hopx, LCN2, mCherry, Mcm7, NGF, NGFR, proBDNF, pTau-S199, or Slc22A17) were diluted in PBS together with 3% Goat/donkey serum and 0.3% Tween 20 and incubated overnight at 4ºC with the sections. This was followed by washing with PBS 3 times within an hour and incubating for four hours at room temperature with the correct secondary antibody conjugated with a desired fluorophore. After short wash samples are then incubated in 4,6-diamidino-2-phenylindole (DAPI) diluted in PBS for 15 minutes. Additional steps of washing were done and samples are mounted on the charged glass slides. After mounting slides are left to dry and covered with a coverslip using Aqua-Poly/Mount (Polysciences Europe GmbH). Human: paraffin-embedded tissue section blanks (20-micron thickness) were obtained from New York Brain Bank. Immunohistochemistry was performed as described [40].

Biohybrid-hydrogels: fixed hydrogels were blocked and permeabilized using 10% Goat Serum, 0.3% Tween 20, and 1x PBS solution for one hour at room temperature, followed by primary and secondary antibody treatments (in 3% Goat serum 0.3% Tween 20, and 1x PBS). See table S1 for antibody information, table S2 for information on the human brain samples.

Imaging and Quantifications

Spinning Disc Zeiss Axio Observer.Z1 microscope (Oberkochen, Germany) equipped with ZEN software (version blue edition, v3.2, company, Carl Zeiss, Jena, Germany) was used to acquire the

fluorescence images of the 40-µm thick mouse brain tissue sections (along with the complete ventral dorsal extent of the DG at 20x magnification) and the biohybrid hydrogels (5 images per hydrogel at 10x magnification, image acquisition dimensions were 704, 999, 300 µm, respectively, with a step size of 2 µm). Human brain sections were imaged with Zeiss LSM 800 scanning confocal microscopes with Airyscan super-resolution module (Oberkochen, Germany). Images were analyzed using ZEN (v3.2, Carl Zeiss, Jena, Germany) or ImageJ (v1.53, NIH, Bethesda, MD, USA version, company, city, country, https://imagej.nih.gov/ij/) or Arivis Vision 4D (v4) software. BrdU/GFAP, BrdU/DCX/mCherry, and BrdU/GFAP/mCherry cells were manually counted in every sixth section (240 mm apart) and were normalized to the area (measured via Arivis vision 4D software) of the granular layer of the dentate gyrus present through the ventral dorsal axis of each hemisphere (Fig. 2G, Fig. S2, S3, and S4, Data S4). In the case of morpholino-treated cells injection, BrdU/DCX/mCherry triple-positive cells were manually counted, only the sections with at least one mCherry positive cell in the granular layer were considered for analysis (Fig. 2J). Quantification of amyloid β plaques (4G8 staining) and phosphorylated Tau-S199 was done via intensity measurement (using Zen v3.2 software), the total intensity was normalized to the area dentate gyrus with proper background noise correction (Fig. 3F, 3H, Data S4). Volume analysis of the hydrogel encapsulated GFAP cells and human brain sample images for Lcn2 expression were performed in an automated manner using the Arivis vision 4D pipeline.

Single Cell Sequencing and Analyses

Mouse hippocampi were isolated as described [31] and cells were kept on ice until dissociated into cells which were used for the single-cell sequencing. Single cell sequencing was performed as described [5, 14, 31]. Sequencing dataset is available on NCBI GEO (https://www.ncbi.nlm.nih.gov/geo/) with accession number GSE189626. We performed all analyses with R.4.0 and Seurat V4. A Seurat object was generated for each dataset, the data were normalized with NormalizeData and 500-2000 variable genes were identified. Data were scaled and nCount_RNA (nUMI) were regressed out. The first 20 PCA were determined, clusters were identified using resolution of 1 and UMAP was calculated for 2D visualization. Data scaling, cluster identification and UMAP detection was performed as described before [14]. To identify main cell types, we used known marker genes and top marker gene of each cluster. The marker genes were identified using the Seurat function "FindAllMarkers" with only.pos = T. Then, top 20 markers of each cluster were identified and heatmaps were generated. Human organoid, fetal brain and adult brain single cell sequencing clustering, heat map generation and tSNE plots were generated as described [5, 13].

NanoString GeoMx digital spatial profiling (DSP)

Using DSP, we performed a multiplexed and spatially resolved profiling analysis on Lv16-p6NST90-hUb-mNGFR-T2A-mCherry and Lv13-p6NST90-hUb-mCherry injected contralateral hemispheres of WT and APP mice. DSP technology uses antibodies with UV photocleavable indexing oligos for protein profiling within the selected regions of interest (ROIs). Using the slide preparation protocol from NanoString Technologies, Inc (Seattle, WA, USA), 5-µm-thick FFPE sections of WT and APP mice brains were prepared from the viral injected site. Morphology markers for visualizing the neural cells (GFAP, AF594), immune cells (Iba1, AF647), mCherry (AF532), and nucleic acids (AF488), were applied for 1 h at room temperature prior to being loaded on the GeoMx Digital Spatial Profiler (NanoString Technologies, Inc). As shown in Fig. 3A, based on fluorescence imaging, ROIs (200–600 µm in diameter) within the DG areas were

chosen for multiplex profiling. The DSP exposed each ROI to a 385-nm light to release the indexing oligos, and the photocleaved oligos were transferred into a microwell. The DSP sequencing data were processed using the GeoMx DSP analysis suite (GEOMX-B0007). Reads were normalized to signal-to-noise ratio (Fig. 3B, Data S7 and S8).

Statistical Analyses

Data analysis was performed using Prism software (Version 8, GraphPad Software, Inc). Results were expressed as mean ± standard deviation (SD). Statistical significance was determined using a Student's t test when the experiment contained two groups, an ANOVA when comparing more than two groups, or a one-sample t test when comparing to a hypothetical value. Bonferroni and Tukey's post hoc tests were performed and mentioned in the text wherever applicable. The level of conventional statistical significance was set at $p < 0.05$ and displayed visually as * $p < 0.05$, ** $p < 0.01$, and *** $p < 0.001$.

**Abbreviations**

| | |
|---|---|
| AD: | Alzheimer's disease |
| ANOVA: | Analysis of variance |
| APP: | Amyloid precursor protein |
| Aβ42: | Amyloid-β 42 |
| BDNF: | Brain-derived neurotrophic factor |
| BrdU: | Bromodeoxyuridine |
| DAPI: | 4′,6-diamidino-2-phenylindole |
| Dcx: | Doublecortin |
| DEG: | Differentially expressed gene |
| DG: | Dentate gyrus |
| GFAP: | Glial fibrillary acidic protein |
| Lcn2: | Lipocalin-2 |
| LV: | Lentivirus |
| NGFR: | Nerve growth factor receptor |
| PS1: | Presenilin 1 |
| SGZ: | Subgranular zone |
| Slc22a17: | Solute carrier protein 22 a 17 |
| tSNE: | t-distributed stochastic neighbor embedding |

**Declarations**

**Ethical Approval**

All animal experiments were performed in accordance with the applicable European regulations and approved by the responsible authority (Landesdirektion Sachsen Germany and TU Dresden-Kommission für Tierversuche) under license number TVV 87/2016. Animals were handled with extreme precaution to reduce suffering and overall animal numbers. Human brain samples were obtained from New York Brain Bank within institutional regulations of Columbia University.

**Consent to participate**

Not applicable.

## Consent for publication

Not applicable.

## Availability of supporting data

All data and relevant accession numbers are available in the main text or the supplementary materials. Raw data for mouse single cell sequencing is available on GEO (accession number GSE189626). Supplementary Materials: Figs. S1 to S7, Tables S1 to S2, Data S1 to S8.

## Competing interests

CK is the chief executive officer of Neuron-D GmbH, which did not have any influence on or contribution to the design and execution of this study. Other authors declare no competing interests.

## Funding

This work was supported by German Center for Neurodegenerative Disease (DZNE) and Columbia University Schaefer Research Scholar Award (CK).

## Authors' contributions

Conceptualization: TS, CK; Experimental materials/procedures: TS, SP, PB, ISM, GT, CK; Data acquisition: TS, PB, CK; Data analyses: TS, MIC, PB, GT, CK; Funding: CK; Writing the manuscript: TS, CK; All authors contributed to editing of the manuscript. All authors read and approved the final manuscript.

## Acknowledgments

We would like to thank DRESDEN-Concept Genome Center and the deep sequencing facility, BioDIP Biopolis Dresden imaging platform and histology facility, Taub Institute for Research on Alzheimer's Disease and the Aging Brain Imaging Platform, New York Brain Bank, and Molecular Pathology platform of the Columbia University Herbert Irving Comprehensive Cancer Center for technical help and New York Brain Bank for post-mortem human brain sections. We would like to thank Dr. Michael L. Shelanski for critical comments on the manuscript.

**Authors' information**

**German Center for Neurodegenerative Diseases (DZNE) within Helmholtz Association; 01307, Dresden, Germany**

Tohid Siddiqui, Mehmet Ilyas Cosacak, Stanislava Popova, Prabesh Bhattarai &Caghan Kizil

**Department of Neurology, Columbia University Irving Medical Center; New York, NY 10032, USA**

Prabesh Bhattarai, Giuseppe Tosto &Caghan Kizil

**Taub Institute for Research on Alzheimer's Disease and the Aging Brain, Columbia University Irving Medical Center; New York, NY 10032, USA**

Prabesh Bhattarai, Ismael Santa-Maria, Giuseppe Tosto &Caghan Kizil

**Department of Pathology and Cell Biology, Columbia University Irving Medical Center; New York, NY 10032, USA**

Ismael Santa-Maria

**References**

1 Angelastro JM, Klimaschewski L, Tang S, Vitolo OV, Weissman TA, Donlin LT, Shelanski ML, Greene LA (2000) Identification of diverse nerve growth factor-regulated genes by serial analysis of gene expression (SAGE) profiling. Proc Natl Acad Sci U S A 97: 10424-10429 Doi 10.1073/pnas.97.19.10424

2 Arber C, Lovejoy C, Harris L, Willumsen N, Alatza A, Casey JM, Lines G, Kerins C, Mueller AK, Zetterberg Het al (2021) Familial Alzheimer's Disease Mutations in PSEN1 Lead to Premature Human Stem Cell Neurogenesis. Cell Rep 34: 108615 Doi 10.1016/j.celrep.2020.108615

3 Artegiani B, Lindemann D, Calegari F (2011) Overexpression of cdk4 and cyclinD1 triggers greater expansion of neural stem cells in the adult mouse brain. J Exp Med 208: 937-948 Doi 10.1084/jem.20102167

4 Betten R, Scharner B, Probst S, Edemir B, Wolff NA, Langelueddecke C, Lee WK, Thevenod F (2018) Tonicity inversely modulates lipocalin-2 (Lcn2/24p3/NGAL) receptor (SLC22A17) and Lcn2 expression via Wnt/beta-catenin signaling in renal inner medullary collecting duct cells: implications for cell fate and bacterial infection. Cell Commun Signal 16: 74 Doi 10.1186/s12964-018-0285-3

5 Bhattarai P, Cosacak MI, Mashkaryan V, Demir S, Popova S, Govindarajan N, Brandt K, Zhang Y, Chang W, Ampatzis Ket al (2020) Neuron-glia interaction through Serotonin-BDNF-NGFR axis enables regenerative neurogenesis in Alzheimer's model of adult zebrafish brain. . PLoS Biol 18: e3000585 Doi 10.1371/journal.pbio.3000585.

6 Bhattarai P, Thomas AK, Cosacak MI, Papadimitriou C, Mashkaryan V, Zhang Y, Kizil C (2017) Modeling Amyloid-β42 Toxicity and Neurodegeneration in Adult Zebrafish Brain. Journal of Visualized Experiments 128: Doi 10.3791/56014

7 Bhattarai P, Thomas AK, Papadimitriou C, Cosacak MI, Mashkaryan V, Froc C, Kurth T, Dahl A, Zhang Y, Kizil C (2016) IL4/STAT6 signaling activates neural stem cell proliferation and neurogenesis upon Amyloid-β42 aggregation in adult zebrafish brain. Cell Reports 17: 941–948 Doi 10.1016/j.celrep.2016.09.075

8 Blurton-Jones M, Kitazawa M, Martinez-Coria H, Castello NA, Müller F-J, Loring JF, Yamasaki TR, Poon WW, Green KN, LaFerla FM (2009) Neural stem cells improve cognition via BDNF in a transgenic model of Alzheimer disease. Proceedings of the National Academy of Sciences of the United States of America 106: 13594-13599 Doi 10.1073/pnas.0901402106
9 Casse F, Richetin K, Toni N (2018) Astrocytes' Contribution to Adult Neurogenesis in Physiology and Alzheimer's Disease. Front Cell Neurosci 12: 432 Doi 10.3389/fncel.2018.00432
10 Choi SH, Bylykbashi E, Chatila ZK, Lee SW, Pulli B, Clemenson GD, Kim E, Rompala A, Oram MK, Asselin Cet al (2018) Combined adult neurogenesis and BDNF mimic exercise effects on cognition in an Alzheimer's mouse model. Science 361: Doi 10.1126/science.aan8821
11 Choi SH, Tanzi RE (2019) Is Alzheimer's Disease a Neurogenesis Disorder? Cell stem cell 25: 7-8 Doi 10.1016/j.stem.2019.06.001
12 Cosacak MI, Bhattarai P, De Jager PL, Menon V, Tosto G, Kizil C (2022) Single Cell/Nucleus Transcriptomics Comparison in Zebrafish and Humans Reveals Common and Distinct Molecular Responses to Alzheimer's Disease. Cells 11: 1807 Doi https://doi.org/10.3390/cells11111807
13 Cosacak MI, Bhattarai P, Kizil C (2020) Alzheimer's disease, neural stem cells and neurogenesis: cellular phase at single-cell level. Neural Reg Res 15: 824-827 Doi 10.4103/1673-5374.268896
14 Cosacak MI, Bhattarai P, Reinhardt S, Petzold A, Dahl A, Zhang Y, Kizil C (2019) Single-Cell Transcriptomics Analyses of Neural Stem Cell Heterogeneity and Contextual Plasticity in a Zebrafish Brain Model of Amyloid Toxicity. Cell Rep 27: 1307-1318 e1303 Doi 10.1016/j.celrep.2019.03.090
15 Cosacak MI, Papadimitriou C, Kizil C (2015) Regeneration, Plasticity, and Induced Molecular Programs in Adult Zebrafish Brain. Biomed Res Int 2015:769763:
16 De Vincenti AP, Rios AS, Paratcha G, Ledda F (2019) Mechanisms That Modulate and Diversify BDNF Functions: Implications for Hippocampal Synaptic Plasticity. Front Cell Neurosci 13: 135 Doi 10.3389/fncel.2019.00135
17 Dzamba D, Harantova L, Butenko O, Anderova M (2016) Glial cells - the key elements of Alzheimer´s disease. Curr Alzheimer Res:
18 Eze UC, Bhaduri A, Haeussler M, Nowakowski TJ, Kriegstein AR (2021) Single-cell atlas of early human brain development highlights heterogeneity of human neuroepithelial cells and early radial glia. Nat Neurosci 24: 584-594 Doi 10.1038/s41593-020-00794-1
19 Ho YP, Schnabel V, Swiersy A, Stirnnagel K, Lindemann D (2012) A small-molecule-controlled system for efficient pseudotyping of prototype foamy virus vectors. Mol Ther 20: 1167-1176 Doi 10.1038/mt.2012.61
20 Huang EJ, Reichardt LF (2003) Trk receptors: roles in neuronal signal transduction. Annu Rev Biochem 72: 609-642 Doi 10.1146/annurev.biochem.72.121801.161629
21 Ishii A, Katsuura G, Imamaki H, Kimura H, Mori KP, Kuwabara T, Kasahara M, Yokoi H, Ohinata K, Kawanishi Tet al (2017) Obesity-promoting and anti-thermogenic effects of neutrophil gelatinase-associated lipocalin in mice. Sci Rep 7: 15501 Doi 10.1038/s41598-017-15825-4

22 Jiang J, Wang C, Qi R, Fu H, Ma Q (2020) scREAD: A Single-Cell RNA-Seq Database for Alzheimer's Disease. iScience 23: 101769 Doi 10.1016/j.isci.2020.101769
23 Jurisch-Yaksi N, Yaksi E, Kizil C (2020) Radial glia in the zebrafish brain: Functional, structural, and physiological comparison with the mammalian glia. Glia: Doi 10.1002/glia.23849
24 Kizil C, Bhattarai P (2018) Is Alzheimer's Also a Stem Cell Disease? - The Zebrafish Perspective. Front Cell Dev Biol 6: 159 Doi 10.3389/fcell.2018.00159
25 Kizil C, Kaslin J, Kroehne V, Brand M (2012) Adult neurogenesis and brain regeneration in zebrafish. Dev Neurobiol 72: 429-461 Doi 10.1002/dneu.20918
26 Kizil C, Sariya S, Kim YA, Rajabli F, Martin E, Reyes-Dumeyer D, Vardarajan B, Maldonado A, Haines JL, Mayeux Ret al (2022) Admixture Mapping of Alzheimer's disease in Caribbean Hispanics identifies a new locus on 22q13.1. Mol Psychiatry: Doi 10.1038/s41380-022-01526-6
27 Kronenberg G, Reuter K, Steiner B, Brandt MD, Jessberger S, Yamaguchi M, Kempermann G (2003) Subpopulations of proliferating cells of the adult hippocampus respond differently to physiologic neurogenic stimuli. J Comp Neurol 467: 455-463 Doi 10.1002/cne.10945
28 Lee AJ, Raghavan NS, Bhattarai P, Siddiqui T, Sariya S, Reyes-Dumeyer D, Flowers XE, Cardoso SAL, De Jager PL, Bennett DAet al (2022) FMNL2 regulates gliovascular interactions and is associated with vascular risk factors and cerebrovascular pathology in Alzheimer’s disease. Acta neuropathologica: Doi 10.1007/s00401-022-02431-6
29 Lee S, Park JY, Lee WH, Kim H, Park HC, Mori K, Suk K (2009) Lipocalin-2 is an autocrine mediator of reactive astrocytosis. J Neurosci 29: 234-249 Doi 10.1523/JNEUROSCI.5273-08.2009
30 Llorens F, Hermann P, Villar-Pique A, Diaz-Lucena D, Nagga K, Hansson O, Santana I, Schmitz M, Schmidt C, Varges Det al (2020) Cerebrospinal fluid lipocalin 2 as a novel biomarker for the differential diagnosis of vascular dementia. Nat Commun 11: 619 Doi 10.1038/s41467-020-14373-2
31 Mashkaryan V, Siddiqui T, Popova S, Cosacak MI, Bhattarai P, Brandt K, Govindarajan N, Petzold A, Reinhardt S, Dahl Aet al (2020) Type 1 Interleukin-4 signaling obliterates mouse astroglia in vivo but not in vitro Frontiers in Cell and Developmental Biology 8: 114 Doi 10.3389/fcell.2020.00114
32 Maurage CA, Sergeant N, Ruchoux MM, Hauw JJ, Delacourte A (2003) Phosphorylated serine 199 of microtubule-associated protein tau is a neuronal epitope abundantly expressed in youth and an early marker of tau pathology. Acta neuropathologica 105: 89-97 Doi 10.1007/s00401-002-0608-7
33 Moreno-Jimenez EP, Flor-Garcia M, Terreros-Roncal J, Rabano A, Cafini F, Pallas-Bazarra N, Avila J, Llorens-Martin M (2019) Adult hippocampal neurogenesis is abundant in neurologically healthy subjects and drops sharply in patients with Alzheimer's disease. Nat Med 25: 554-560 Doi 10.1038/s41591-019-0375-9
34 Nykjaer A, Willnow TE, Petersen CM (2005) p75NTR--live or let die. Curr Opin Neurobiol 15: 49-57 Doi 10.1016/j.conb.2005.01.004
35 Papadimitriou C, Celikkaya H, Cosacak MI, Mashkaryan V, Bray L, Bhattarai P, Brandt K, Hollak H, Chen X, He Set al (2018) 3D Culture Method for Alzheimer's Disease Modeling Reveals Interleukin-4 Rescues Abeta42-Induced Loss of Human Neural Stem Cell Plasticity. Dev Cell 46: 85-101 e108 Doi 10.1016/j.devcel.2018.06.005

36 Stern Y (2012) Cognitive reserve in ageing and Alzheimer's disease. The Lancet Neurology 11: 1006-1012 Doi 10.1016/S1474-4422(12)70191-6
37 Stirnnagel K, Luftenegger D, Stange A, Swiersy A, Mullers E, Reh J, Stanke N, Grosse A, Chiantia S, Keller Het al (2010) Analysis of prototype foamy virus particle-host cell interaction with autofluorescent retroviral particles. Retrovirology 7: 45 Doi 10.1186/1742-4690-7-45
38 Tanaka EM, Ferretti P (2009) Considering the evolution of regeneration in the central nervous system. Nat Rev Neurosci 10: 713-723 Doi 10.1038/nrn2707
39 Terreros-Roncal J, Moreno-Jimenez EP, Flor-Garcia M, Rodriguez-Moreno CB, Trinchero MF, Cafini F, Rabano A, Llorens-Martin M (2021) Impact of neurodegenerative diseases on human adult hippocampal neurogenesis. Science: eabl5163 Doi 10.1126/science.abl5163
40 Waldvogel HJ, Curtis MA, Baer K, Rees MI, Faull RL (2006) Immunohistochemical staining of post-mortem adult human brain sections. Nat Protoc 1: 2719-2732 Doi 10.1038/nprot.2006.354
41 Walker DG, Dalsing-Hernandez JE, Campbell NA, Lue L-F (2009) Decreased expression of CD200 and CD200 receptor in Alzheimer's disease: a potential mechanism leading to chronic inflammation. Experimental neurology 215: 5-19 Doi 10.1016/j.expneurol.2008.09.003
42 Walker TL, Kempermann G (2014) One mouse, two cultures: isolation and culture of adult neural stem cells from the two neurogenic zones of individual mice. J Vis Exp: e51225 Doi 10.3791/51225
43 Wu G, Feder A, Cohen H, Kim JJ, Calderon S, Charney DS, Mathe AA (2013) Understanding resilience. Front Behav Neurosci 7: 10 Doi 10.3389/fnbeh.2013.00010
44 Wyss-Coray T, Loike JD, Brionne TC, Lu E, Anankov R, Yan F, Silverstein SC, Husemann J (2003) Adult mouse astrocytes degrade amyloid-beta in vitro and in situ. Nat Med 9: 453-457 Doi 10.1038/nm838 [pii]
45 Yamada Y, Miyamoto T, Kashima H, Kobara H, Asaka R, Ando H, Higuchi S, Ida K, Shiozawa T (2016) Lipocalin 2 attenuates iron-related oxidative stress and prolongs the survival of ovarian clear cell carcinoma cells by up-regulating the CD44 variant. Free Radic Res 50: 414-425 Doi 10.3109/10715762.2015.1134795
46 Yamazaki Y, Kanekiyo T (2017) Blood-Brain Barrier Dysfunction and the Pathogenesis of Alzheimer's Disease. Int J Mol Sci 18: Doi 10.3390/ijms18091965
47 Yao XQ, Jiao SS, Saadipour K, Zeng F, Wang QH, Zhu C, Shen LL, Zeng GH, Liang CR, Wang Jet al (2015) p75NTR ectodomain is a physiological neuroprotective molecule against amyloid-beta toxicity in the brain of Alzheimer's disease. Mol Psychiatry 20: 1301-1310 Doi 10.1038/mp.2015.49
48 Young KM, Merson TD, Sotthibundhu A, Coulson EJ, Bartlett PF (2007) p75 neurotrophin receptor expression defines a population of BDNF-responsive neurogenic precursor cells. J Neurosci 27: 5146-5155 Doi 10.1523/JNEUROSCI.0654-07.2007
49 Zhao N, Xu X, Jiang Y, Gao J, Wang F, Xu X, Wen Z, Xie Y, Li J, Li Ret al (2019) Lipocalin-2 may produce damaging effect after cerebral ischemia by inducing astrocytes classical activation. Journal of neuroinflammation 16: 168 Doi 10.1186/s12974-019-1556-7

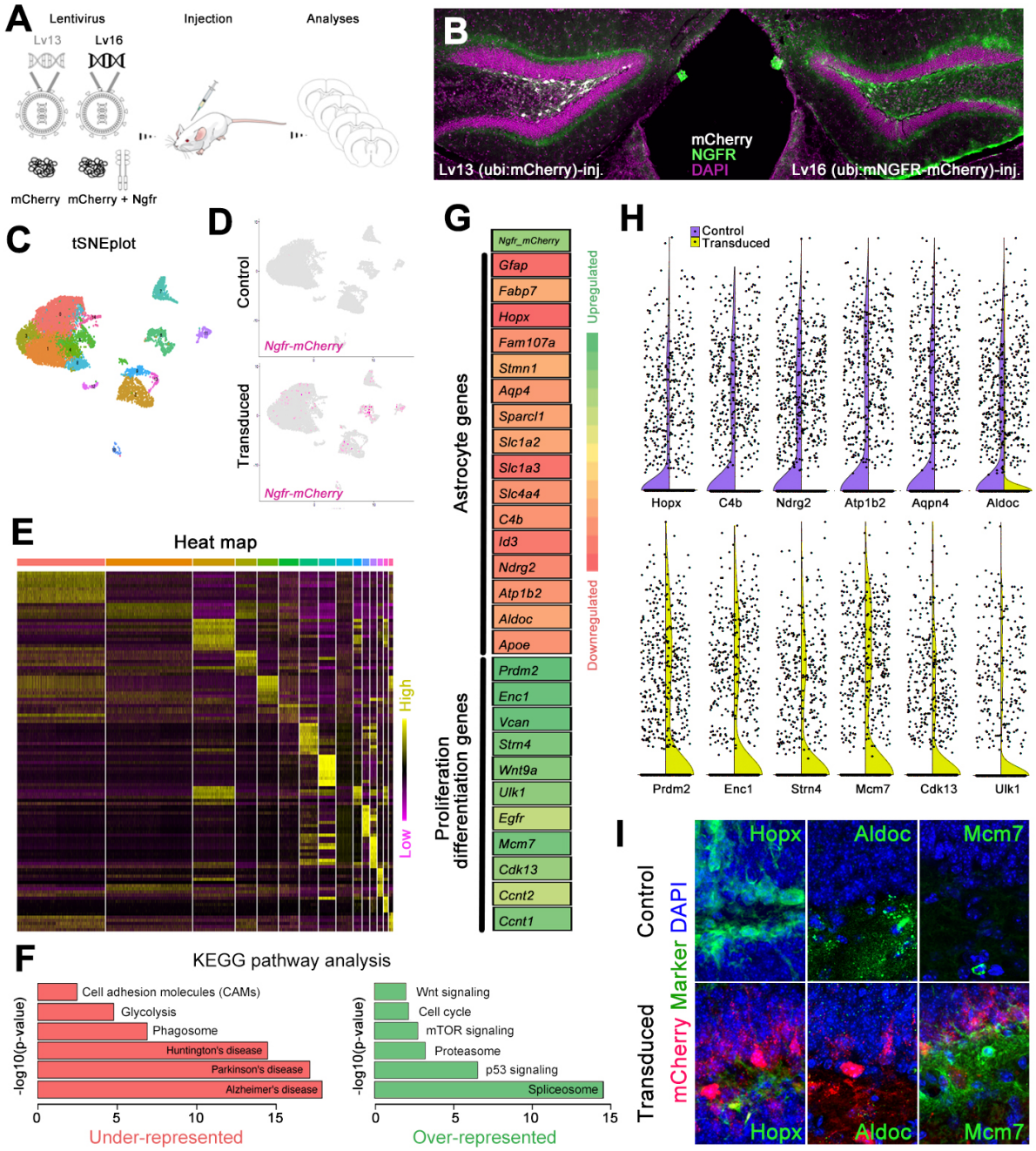


**Fig. 1. NGFR enhances proliferative and neurogenic markers in dentate gyrus (DG) astrocytes. (A)** Schematic strategy for expression lentiviruses: Lv13: mCherry control; Lv16: mCherry-NGFR. **(B)** Cross section images for DGs transduced with Lv13 and Lv16 and immunostained for mCherry, NGFR with DAPI counterstain. Note NGFR expression in the subgranular zone (SGZ) after Lv16 transduction. **(C)** Single cell transcriptomics tSNE plot from dissected DGs after Lv13 and Lv16 transduction. **(D)** tSNE plots from Lv13 and Lv16 transduction showing the expression of Ngfr-mCherry, which is detectable only after Lv16. **(E)** heat map of different cell types. **(F)** KEGG pathway analyses on astrocytic population, showing downregulated

and upregulated pathways. **(G)** A heat map for selected differentially expressed genes (DEGs) after Lv16. Astrocyte markers are downregulated and proliferation/neurogenesis markers are upregulated**.** **(H)** Violin plots for selected genes: purple: control (Lv13); yellow (Lv16). **(I)** Immunostaining for validating the DEGs in control and Lv16-transduced DG. Scale bars equal 50 μm.

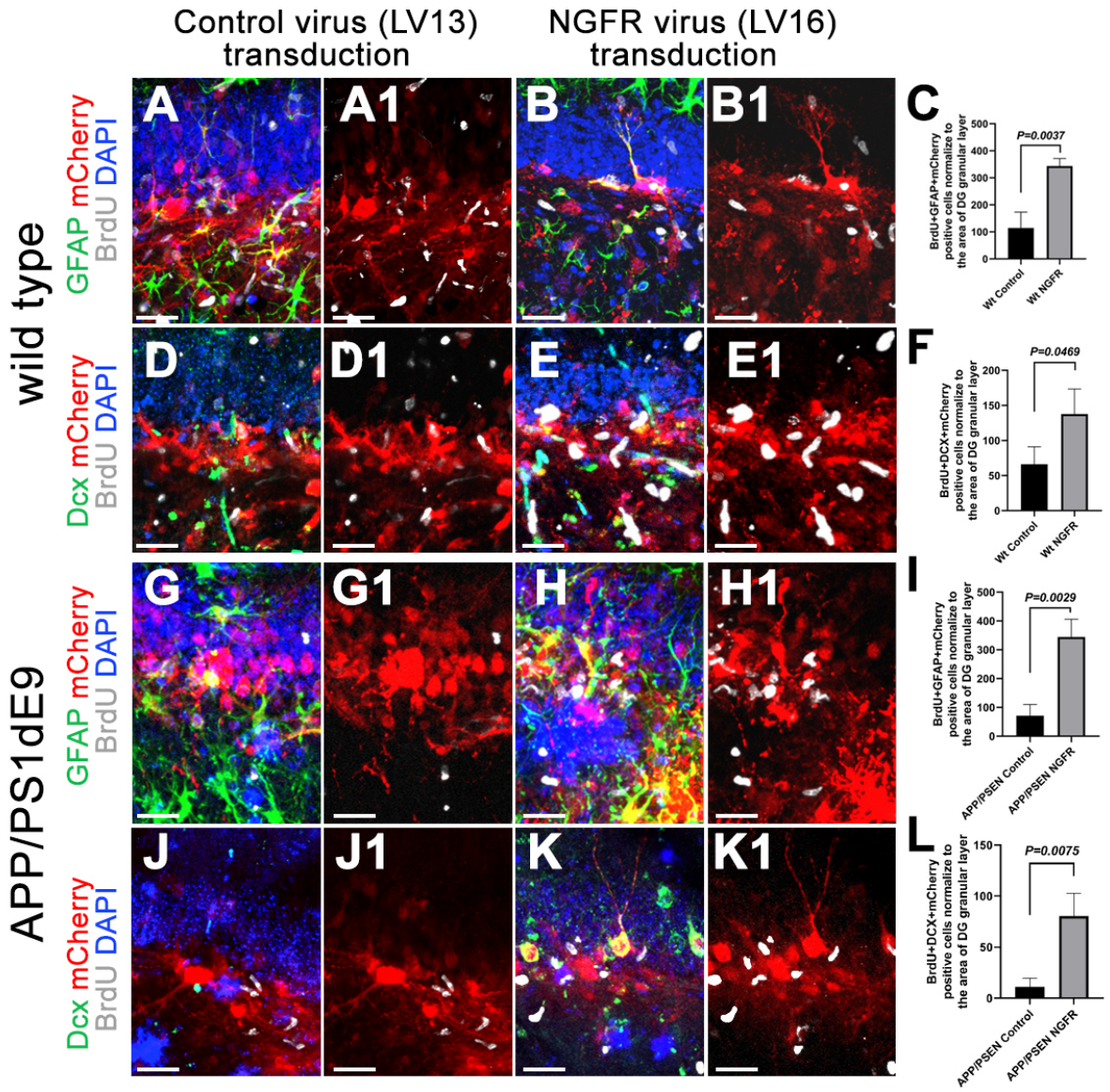


**Fig. 2. NGFR promotes proliferation of DG astrocytes and neurogenesis in wild type and APP/PS1dE9 model of AD. (A, B)** Immunostaining for GFAP, BrdU and mCherry with DAPI counterstain in Lv13- (A) and Lv16- (B) SGZ of wild type mice. **(A1, B1)** BrdU/mCherry channels of A and B. **(C)** Quantification graph for mCherry-BrdU-GFAP triple positive cells. **(D, E)** Immunostaining for Dcx, BrdU and mCherry with DAPI counterstain in Lv13- (A) and Lv16-transduced (B) SGZ. **(D1, E1)** BrdU/mCherry channels of D and E. **(F)** Quantification graph for mCherry-BrdU-Dcx triple positive cells of wild type mice. **(G, H)** Immunostaining for GFAP, BrdU and mCherry with DAPI counterstain in Lv13- (G) and Lv16-transduced (H) SGZ of APP/PS1dE9 mice. **(G1, H1)** BrdU/mCherry channels of G and H. **(I)** Quantification graph for mCherry-BrdU-GFAP triple positive cells. **(J, K)** Immunostaining for Dcx, BrdU and mCherry with DAPI counterstain in Lv13- (J) and Lv16-transduced (K) SGZ of APP/PS1dE9 mice. **(J1, K1)** BrdU/mCherry channels of J and K. **(L)** Quantification graph for mCherry-BrdU-Dcx triple positive cells. Scale bars equal 50 um.

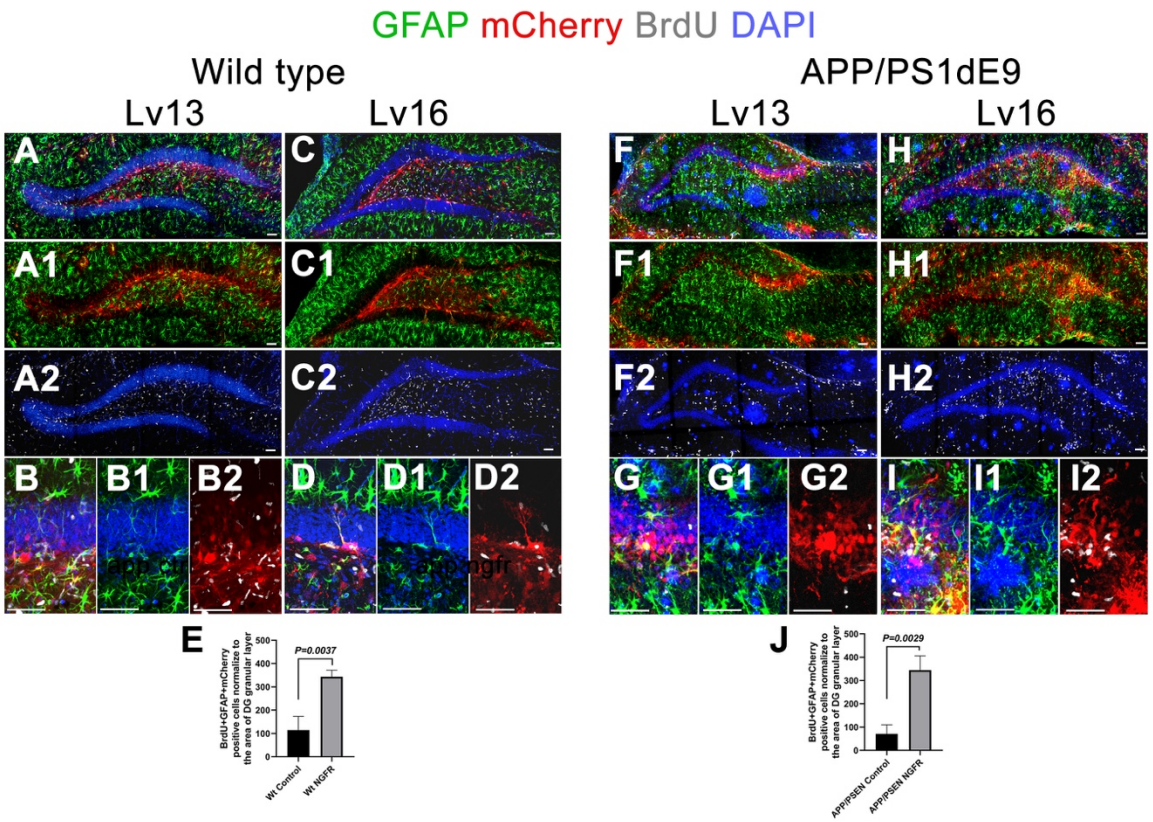


**Fig. 3. Lv16 transduction enhances astroglia proliferation in wild type and APP/PS1dE9 mouse model of Alzheimer's disease. (A)** GFAP, mCherry, BrdU triple immunostaining with DAPI counterstain in Lv13-transduced wild type mouse dentate gyrus. **(A1)** DAPI and BrdU omitted from A. **(A2)** GFAP and mCherry omitted from A. **(B)** Higher magnification image of subgranular zone. **(B1)** BrdU and mCherry omitted from B. **(B2)** GFAP and DAPI omitted from B. **(C)** GFAP, mCherry, BrdU triple immunostaining with DAPI counterstain in Lv16-transduced wild type mouse dentate gyrus. **(C1)** DAPI and BrdU omitted from C. **(C2)** GFAP and mCherry omitted from C. **(D)** Higher magnification image of subgranular zone. **(D1)** BrdU and mCherry omitted from D. **(D2)** GFAP and DAPI omitted from D. **(E)** Quantification graph for BrdU-mCherry-GFAP triple positive cells in Lv13 and Lv16-transduced brains. **(F)** GFAP, mCherry, BrdU triple immunostaining with DAPI counterstain in Lv13-transduced APP/PS1dE9 mouse dentate gyrus. **(F1)** DAPI and BrdU omitted from F. **(F2)** GFAP and mCherry omitted from F**. (G)** Higher magnification image of subgranular zone. **(G1)** BrdU and mCherry omitted from G. **(G2)** GFAP and DAPI omitted from G. **(H)** GFAP, mCherry, BrdU triple immunostaining with DAPI counterstain in Lv16-transduced APP/PS1dE9 mouse dentate gyrus. **(H1)** DAPI and BrdU omitted from H. **(H2)** GFAP and mCherry omitted from H. **(I)** Higher magnification image of subgranular zone. **(I1)** BrdU and mCherry omitted from I. **(I2)** GFAP and DAPI omitted from I. **(J)** Quantification graph for BrdU-mCherry-GFAP triple positive cells in Lv13 and Lv16-transduced brains. Scale bars equal 100 µm.

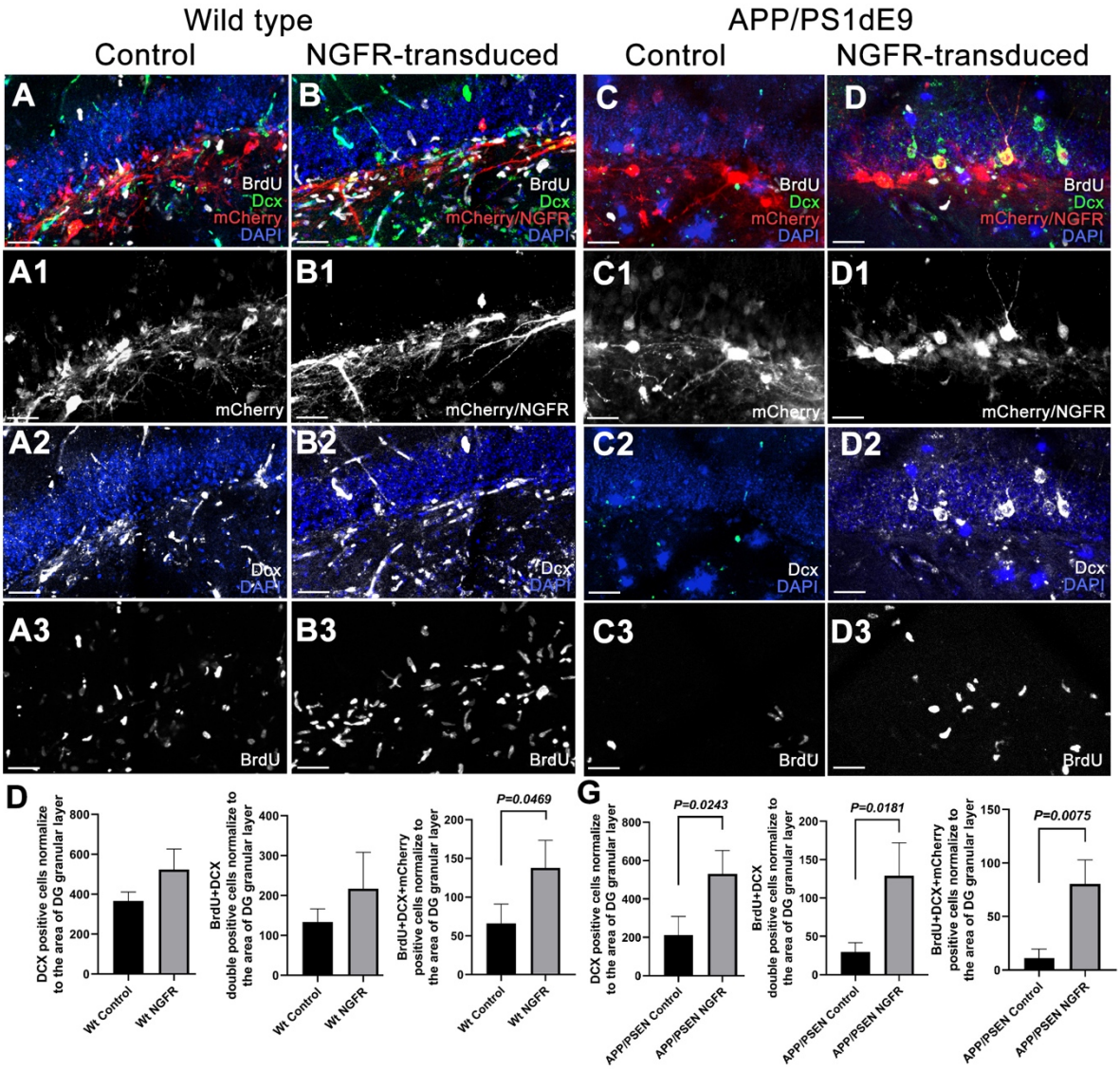


**Fig. 4. Lv16 transduction enhances neurogenesis in wild type and APP/PS1dE9 mouse model of Alzheimer's disease. (A)** Dcx, mCherry, and BrdU triple immunostaining with DAPI counterstain in Lv13-transduced wild type mouse dentate gyrus. **(A1)** mCherry channel of A. **(A2)** Dcx and DAPI channel of A. **(A3)** BrdU channel of A. **(B)** Dcx, mCherry, and BrdU triple immunostaining with DAPI counterstain in Lv16-transduced wild type mouse dentate gyrus. **(B1)** mCherry channel of B. **(B2)** Dcx and DAPI channel of B. **(B3)** BrdU channel of B. **(D)** Normalized values of Dcx-positive, BrdU-Dcx double positive and BrdU-Dcx-mCherry triple positive cells in wild type mouse dentate gyrus transduced with Lv13 (control) or Lv16 (NGFR). **(E)** Dcx, mCherry, BrdU triple immunostaining with DAPI counterstain in Lv13-transduced APP/PS1dE9 mouse dentate gyrus. **(E1)** mCherry channel of e. **(e2)** Dcx and DAPI channel of E. **(E3)** BrdU channel of E. **(F)** Dcx, mCherry, and BrdU triple immunostaining with DAPI counterstain in Lv16-transduced wild type mouse dentate gyrus. **(F1)** mCherry channel of F. **(F2)** Dcx and DAPI channel of F. **(f3)** BrdU channel of F. **(G)** Normalized values of Dcx-positive, BrdU-Dcx double positive and BrdU-Dcx-mCherry triple positive cells in APP/PS1dE9 mouse dentate gyrus transduced with Lv13 (control) or Lv16 (NGFR). Scale bars equal 50 μm.

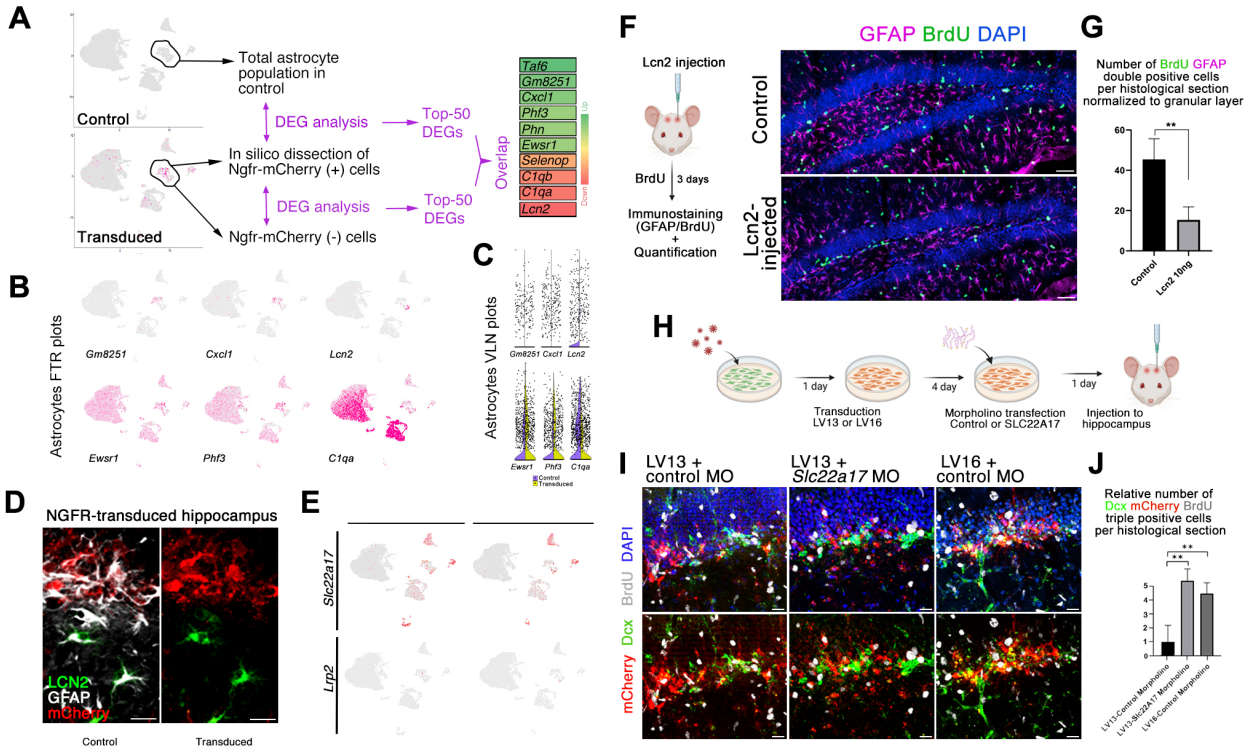


**Fig. 5. NGFR regulates neurogenic response in DG astrocytes through suppression of Lcn2/Slc22a17 activity. (A)** Single cell transcriptomics strategy for isolating NGFR-mCherry positive astrocytes and comparing the transcriptomics profiles to non-transduced astrocytes or control astrocytes. The comparison showed differential expression of 10 genes in common as shown in the heat map. **(B)** Expression of selected genes on tSNE plots. **(C)** Violin plots for selected genes. **(D)** Immunostaining for Lcn2, GFAP and mCherry in LV16 (NGFR)-transduced DG. Lcn2-positive and mCherry positive astrocytes do not overlap. **(E)** tSNE plots for two receptors of Lcn2: *Lrp2, Slc22a17*. **(F)** Injection, BrdU treatment and analyses scheme of the effect of Lcn2 on proliferating GFAP cells, and immunohistochemical staining for BrdU, GFAP and DAPI. **(G)** Quantification graph for BrdU-GFAP double positive cells. **(H)** Schematic representation of the cell-type specific functional knockdown of *Slc22a17* in astrocytes. **(I)** mCherry, Dcx, BrdU immunostaining with DAPI counterstain in SGZs transplanted with Lv13+control morpholino, Lv13+*Slc22a17* morpholino and Lv16+control morpholino-treated astrocytes. Lower panels: DAPI omitted from upper panels **(J)** Quantification of Dcx, mCherry and BrdU triple positive cells in i. Slc22a17 knockdown mimics NGFR transduction. n = 3. Scale bars equal 25 µm.

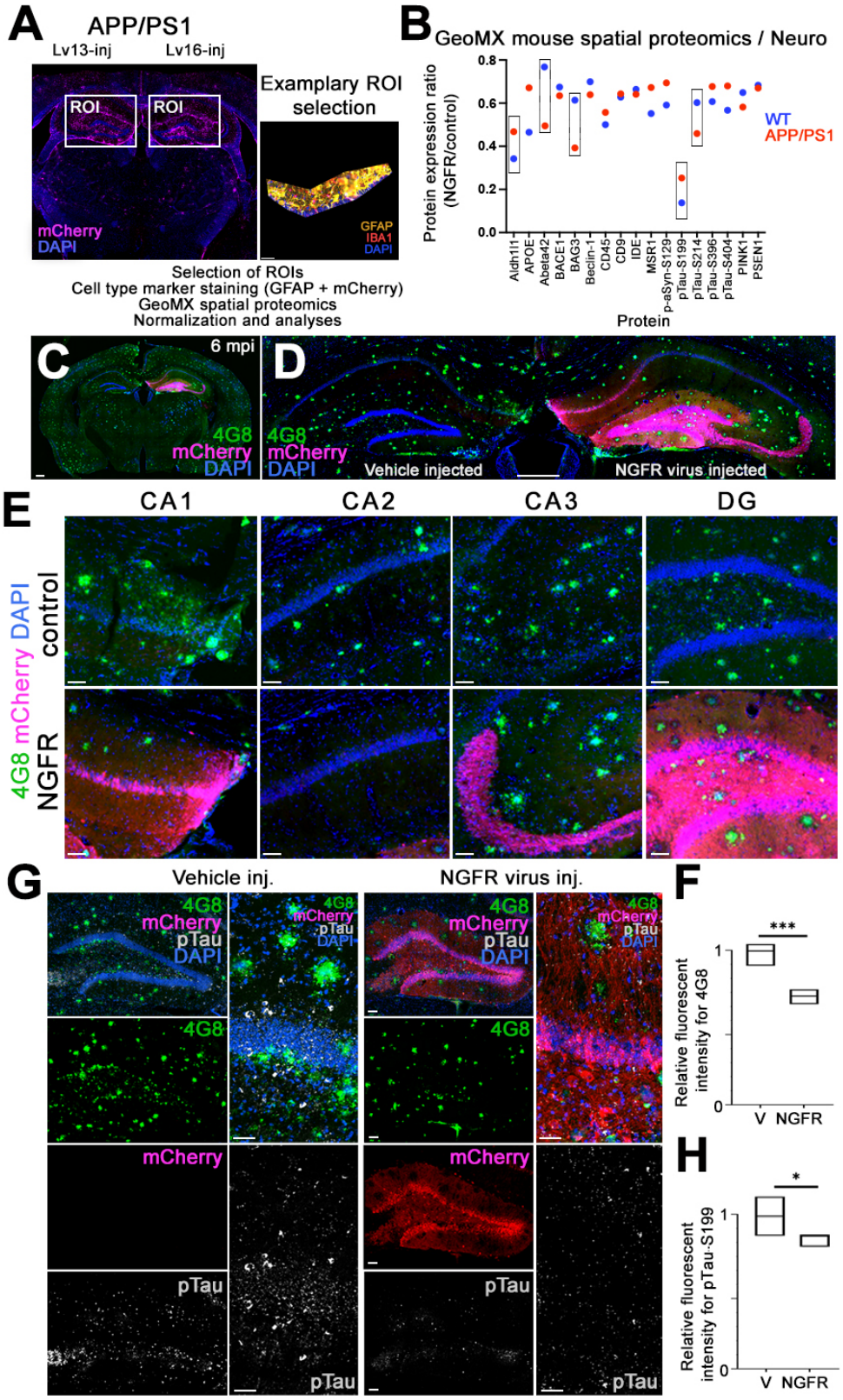
A
APP/PS1
Lv13-inj
Lv16-inj
ROI
ROI
mCherry
DAPI
Examplary ROI selection
GFAP
IBA1
DAPI
Selection of ROIs
Cell type marker staining (GFAP + mCherry)
GeoMX spatial proteomics
Normalization and analyses
B
GeoMX mouse spatial proteomics / Neuro
Protein expression ratio (NGFR/control)
WT
APP/PS1
Aldh1l1
APOE
Abeta42
BACE1
BAG3
Beclin-1
CD45
CD9
IDE
MSR1
p-aSyn-S129
pTau-S199
pTau-S214
pTau-S396
pTau-S404
PINK1
PSEN1
Protein
C
6 mpi
4G8
mCherry
DAPI
D
4G8
mCherry
DAPI
Vehicle injected
NGFR virus injected
E
CA1
CA2
CA3
DG
4G8 mCherry DAPI
control
NGFR
G
Vehicle inj.
NGFR virus inj.
4G8
mCherry
pTau
DAPI
F
***
Relative fluorescent intensity for 4G8
V
NGFR
H
*
Relative fluorescent intensity for pTau-S199
V
NGFR

**Fig. 6. NGFR reduces amyloid-beta42 load and phosphorylated Tau in the hippocampus of APP/PS1dE9 mice. (A)** Representative image from GeoMx spatial proteomics mouse brain section and region of interest (ROI) at the SGZ**. (B)** Plot showing the fold changes of selected proteins upon NGFR transduction in wild type and APP/PS1dE9 mice. **(C)** Representative APP/PS1dE9 mouse brain section immunostained for 4G8 and mCherry with DAPI counterstain at 6 months after transduction with Lv16 in one DG. **(D)** High-magnification image from C**. (E)** Comparison of amyloid load in CA1, CA2, CA3 and DG regions of control and NGFR-transduced hemispheres. **(F)** Quantification of amyloid load in terms of normalized amyloid immunoreactivity by comparing control (v) versus NGFR (Lv16) transduction. n = 5. **(G)** 4G8, mCherry, phosphorylated Tau-S199 immunostaining with DAPI counterstain in control and NGFR-injected DGs. Individual fluorescence channels and close-up images are also shown. **(H)** Quantification of pTau-S199 in terms of normalized fluorescence by comparing control (v) versus NGFR (Lv16) transduction. n = 5. ***: p<0.005, *: p<0.05. Scale bars equal 100 µm.

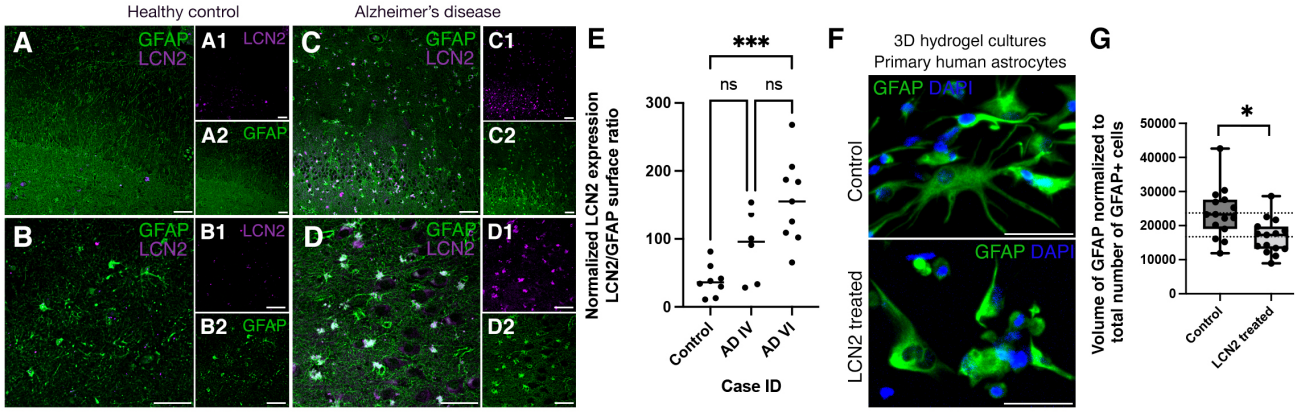


**Fig.7. LCN2 is upregulated in human brains with AD. (A-D)** Immunohistochemical stainings for LCN2 and GFAP on hippocampal brain sections of healthy control (A, B) and Braak stage VI AD patient (C, D). Black-white insets (A1-D2) indicate individual fluorescent channels. LCN2 (top) and GFAP (bottom). **(E)** Quantification of LCN2-positive GFAP cells normalized to total GFAP cells. In total n = 7 human brains, n = 21 images analyzed. ***: p<0.001. **(F)** Immunostaining for GFAP on primary human astrocytes in 3D hydrogels: control and LCN2-treated. **(G)** Quantification of the volume of GFAP normalized to total number of GFAP cells. LCN2-treatment reduces the volume of astroglia, indicative or reactive states. Scale bars equal 50 µm.

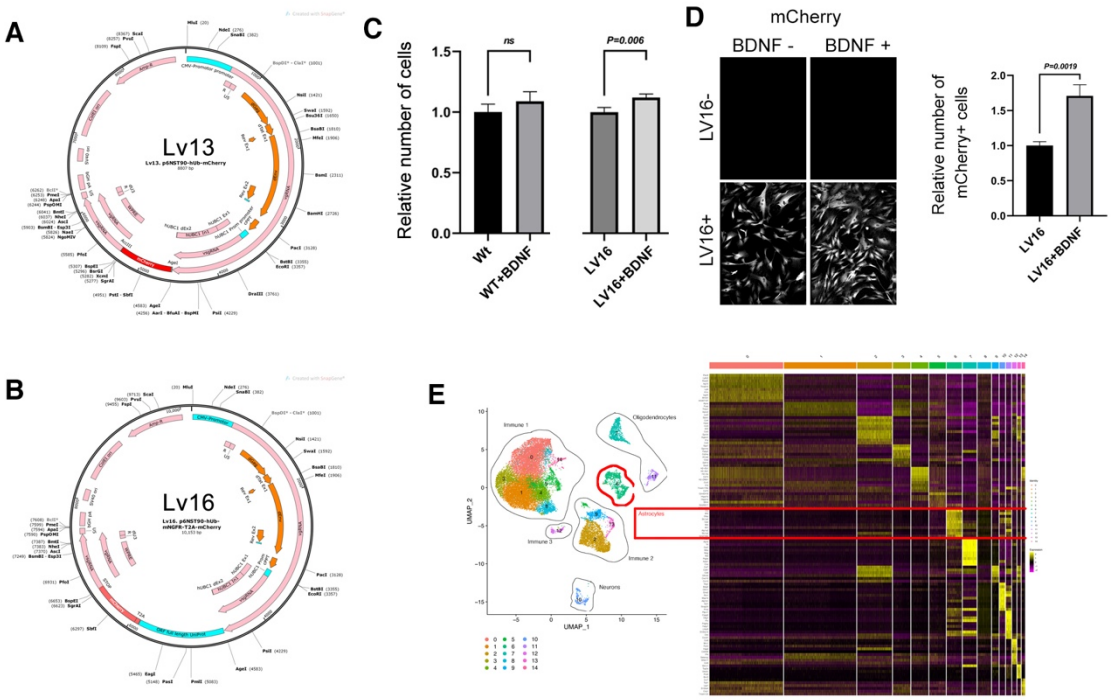


**Fig. S1. Maps of lentiviral vectors, in vitro functionality assay, single cell sequencing heat map. (A)** Lv13: CMV promoter driven mCherry. **(B)** Lv16: CMV promoter-driven mouse NGFR linked to mCherry with T2A self-cleaving peptide. **(C)** Graphs show relative number of cells in culture dish after equi-number seeding of cells that are either untransduced (wt) or LV16-transduced. **(D)** BDNF is added to the culture medium to activate NGFR signalling. Only Lv16-transduced cells are responsive to BDNF. Staining image shows the mCherry -positive cells that increase in response to BDNF and Lv16. Graph indicates the number of mCherry-positive cells after equi-number seeding. **(E)** Single cell sequencing tSNE plot and heat map. Clustering of cells and their cellular identities are shown on the left. Heat map on the right shows the markers for individual cell types and their expression levels. Yellow indicates high expression. Astrocyte population marked with red rectangle.

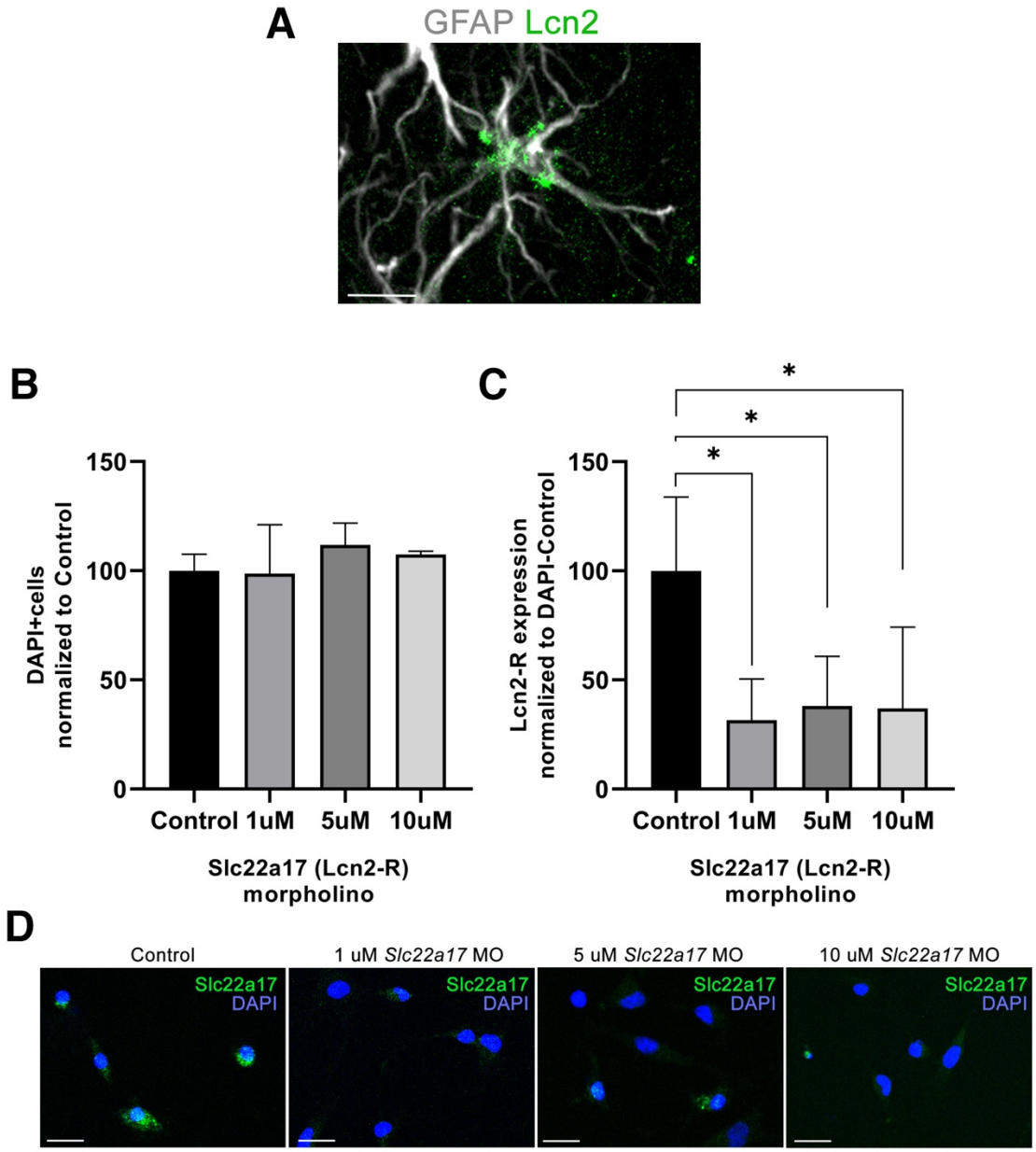


**Fig. S2. Lcn2 expression in astroglia and effectiveness of *Slc22a17* morpholino. (A)** GFAP and Lcn2 double immunolabeling in mouse hippocampus. Scale bars equal 25 µm. **(B)** In vitro cell viability counts in astroglia that are untransfected or transfected with three doses of *Slc22a17* vivo morpholino (1-, 5- and 10 µM). **(C)** Slc22a17 (Lcn2-R) protein expression (fluorescence units on immunolabeled cultures) normalized to DAPI in control and transfected astroglia. **(D)** Slc22a17 immunostaining and DAPI counterstain in control (untransfected) astroglia and astroglia transfected with 1-, 5- and 10 µM vivo morpholino. Scale bars equal 25 µm.

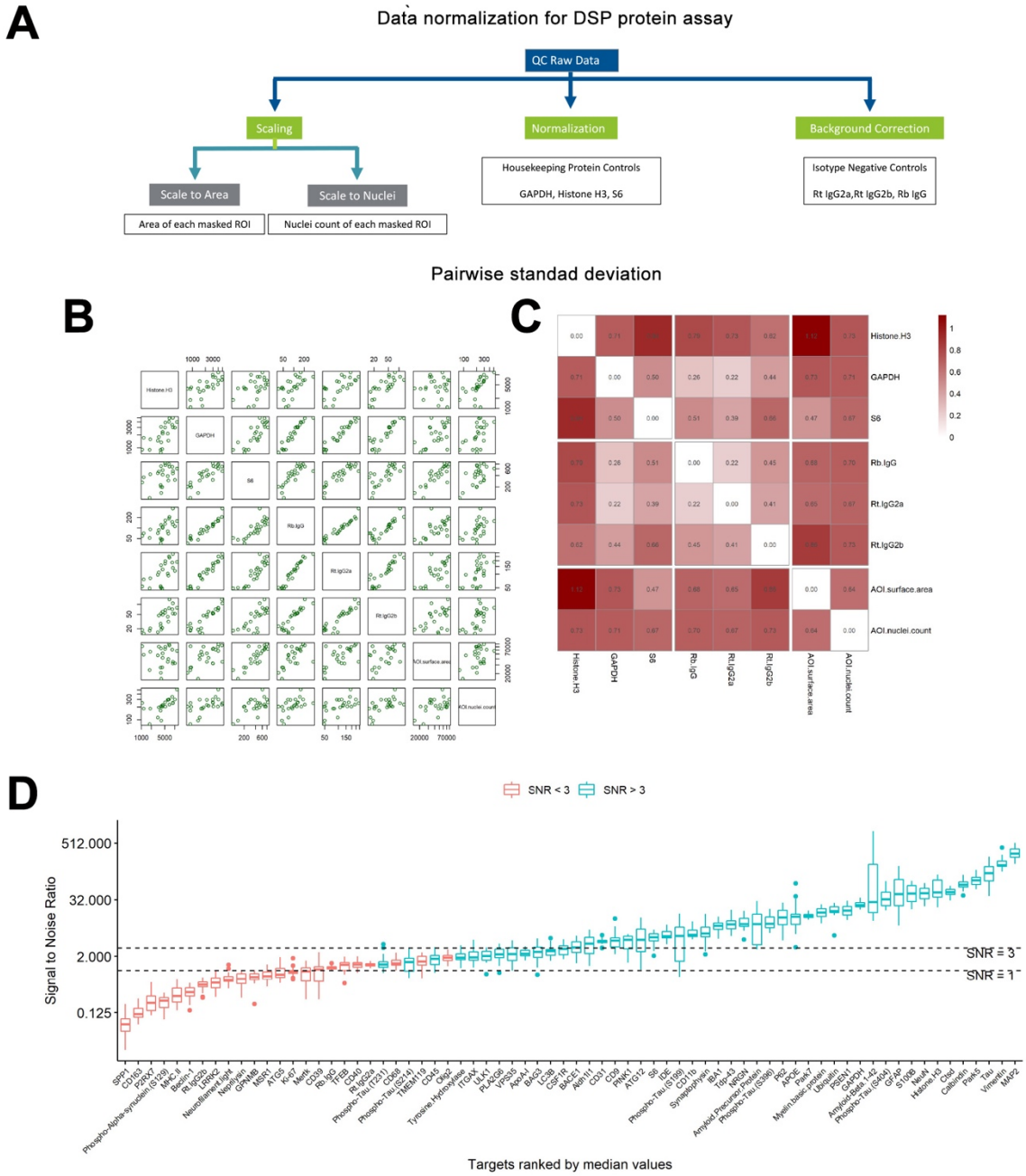


**Fig. S3. Nanostring GeoMX quality control and normalization strategy. (A)** Data normalization options. **(B, C)** Pairwise standard deviation analysis. (B) Raw values plotted for spike-in normalization samples. (C) Standard deviation heat map for surface area, nuclei count, housekeeping genes (Histone H3, GAPDH, S6) or signal-to-noise ratio (IgG, IgG2a, IgG2b). Signal-to-noise ratio normalization has the lowest standard deviation. **(D)** Plot for targets ranked by median expression values normalized to signal-to-noise ratio.

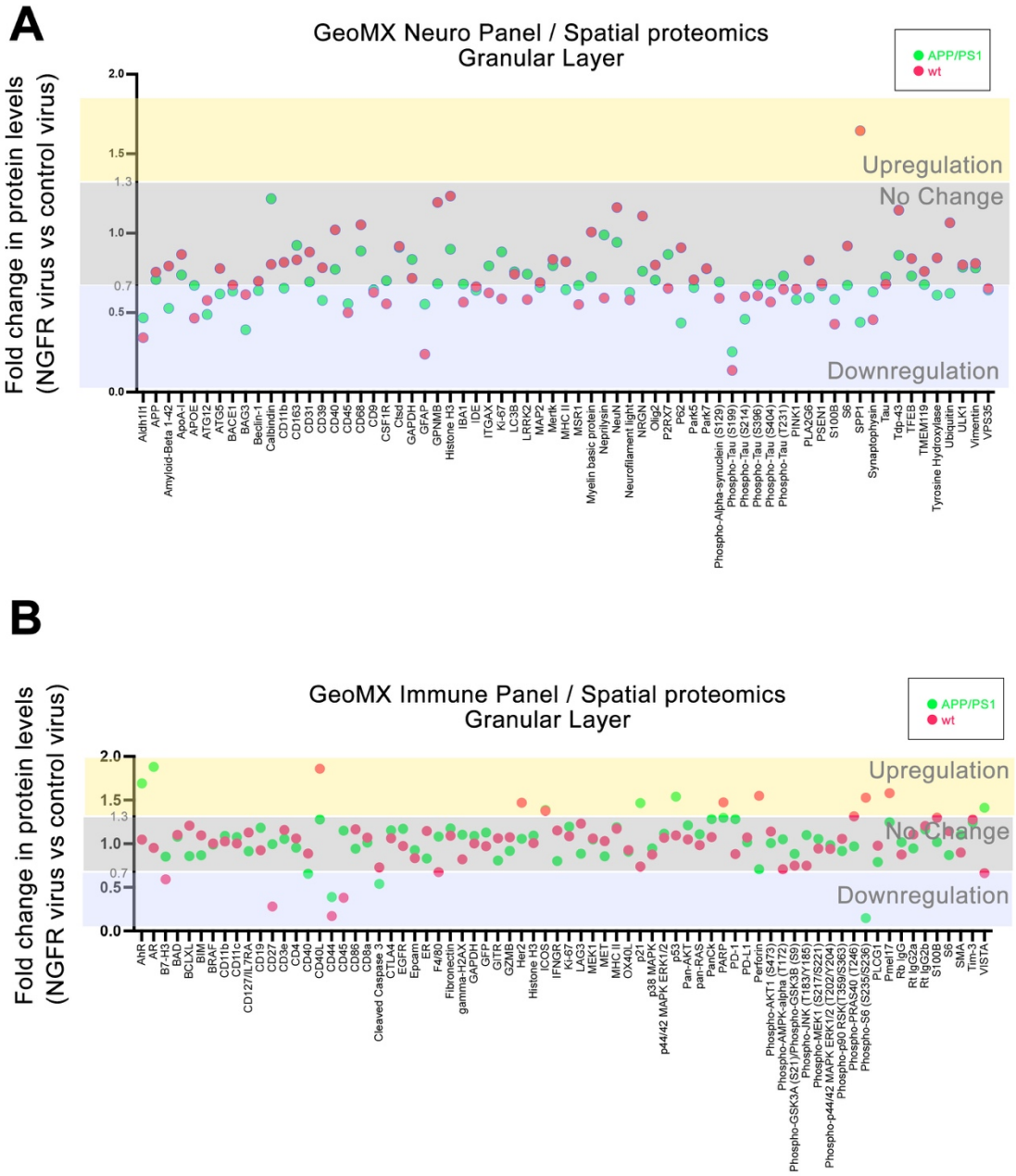


**Fig. S4. GeoMX neuro and immune panel spatial proteomics plot showing fold changes of protein targets in NGFR-transduced brains versus control virus-transduced brains.** Plots indicate targets and their fold changes in wild type animals (red dots) and APP/PS1dE9 mouse model of Alzheimer's disease (green dots). 1.3 and 0.7 are taken as upper and lower boundaries for the no-change criterion. **(A)** Neuro panel. **(B)** Immune panel.

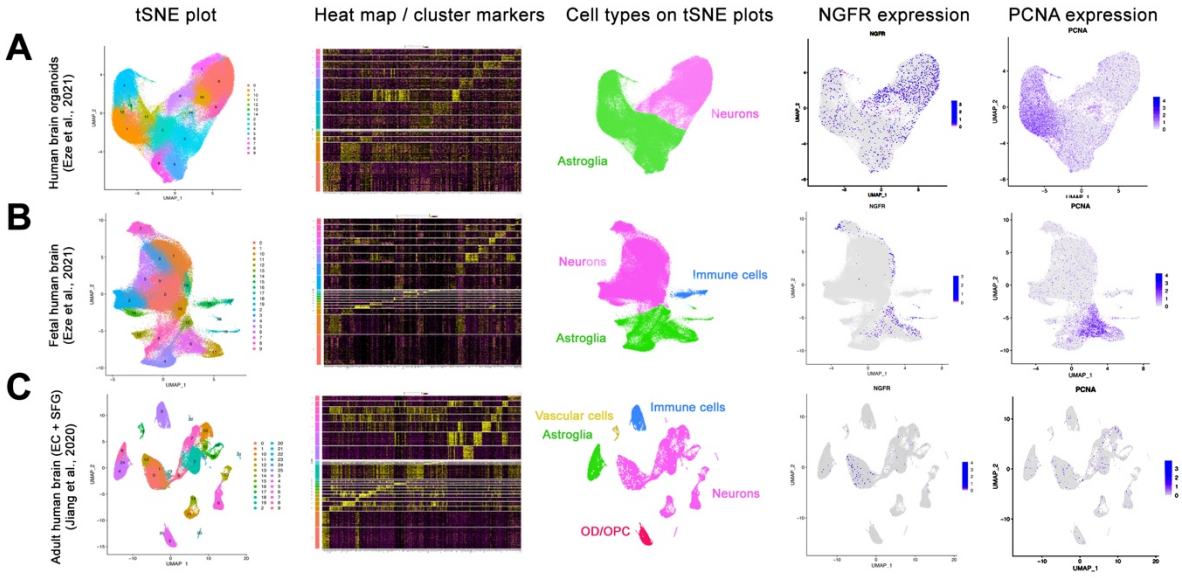


**Fig. S5. Single cell sequencing analyses of human brain organoids, fetal and adult human brains.** tSNE plots for cell clustering, heat maps of top marker genes, identified cell types on colored tSNE plots, tSNE plot for NGFR and PCNA are shown for human datasets of **(A)** human brain organoids, **(B)** fetal human brain, and **(c)** adult human brain entorhinal cortex (EC) and superior frontal gyrus (SFG).

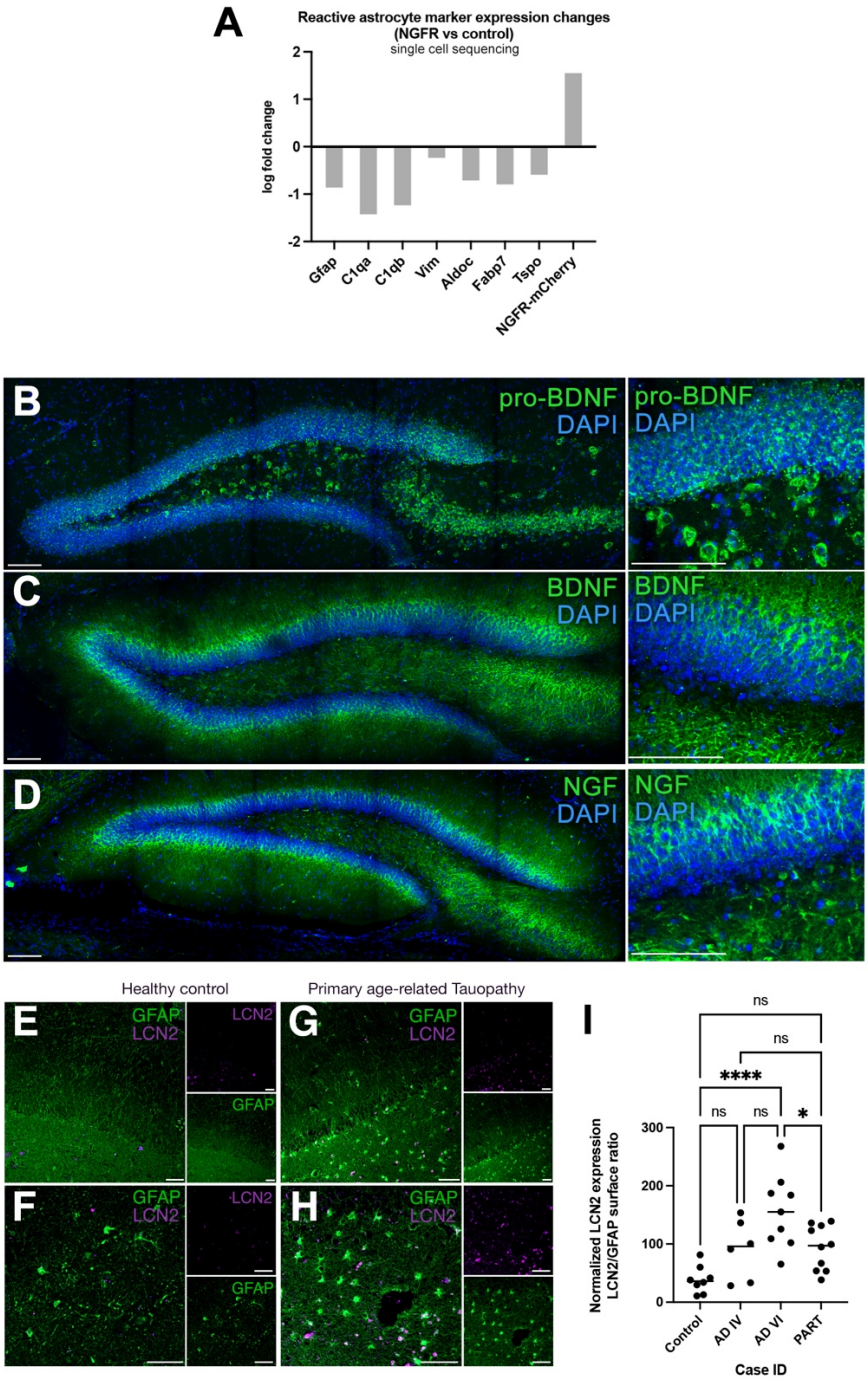


**Fig. S6. Reactive astrocyte markers in single cell transcriptomics, expression of neurotrophins in mouse dentate gyrus (DG), and LCN2 expression in primary age-related Tauopathy patients. (A)** Expression of reactive astrocyte markers GFAP, C1qa, C1qb, Vim, Aldoc, Fabp7, and Tspo are shown. NGFR expression reduces the expression of these markers. NGFR-mCherry expression is shown for comparison. **(B-D)** Expression of pro-BDNF, BDNF and NGF in mouse dentate gyrus. Panels on the right are high magnification from left panels. **(B)** pro-BDNF, **(C)** BDNF, **(D)** NGF. BDNF and NGF are expressed in outer layers of DG, while pro-BDNF is expressed in the subgranular zone and hilus. **(E-H)** Immunohistochemical stainings for

LCN2 and GFAP on hippocampal brain sections of healthy control (E, F; identical to Fig. 4) and primary age-related Tauopathy patient (G, H). Single channel insets to the right of every panel indicate individual fluorescent channels. LCN2 (top) and GFAP (bottom). **(I)** Quantification of LCN2-positive GFAP cells normalized to total GFAP cells. The samples values in Fig. 4 are also included to perform a multiple comparison. In total n = 10 human brains, n = 32 images analyzed. ****: $p<0.0001$. Scale bars equal 25 μm (B-D) and 50 μm (E-H).

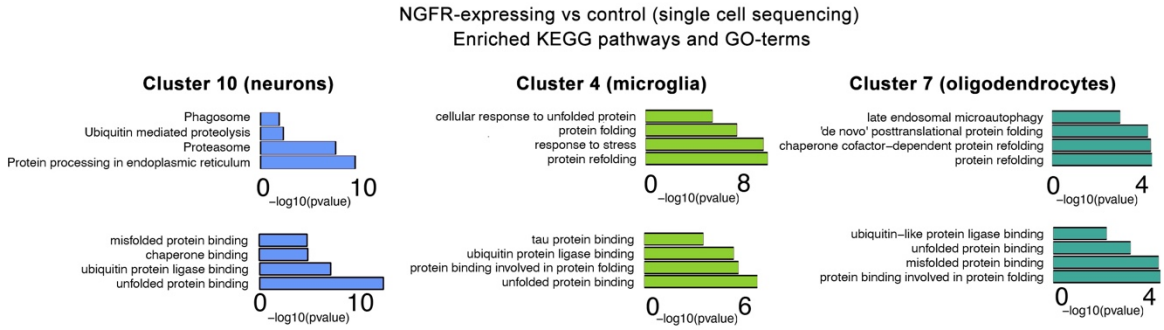


**Fig. S7. Protein clearance and misfolded protein response-related pathways are enriched upon NGFR expression in non-glial cell types.** Differentially expressed genes after NGFR transduction upregulate the pathways related to enhanced protein quality control, toxic protein removal, misfolded protein response in non-neuronal cells. Selected GO-terms and KEGG pathways are depicted.